Sources of particulate-matter air pollution and its oxidative potential in Europe

Kaspar R Daellenbach, Gaëlle Uzu, Jianhui Jiang, Laure-Estelle Cassagnes, Zaira Leni, Athanasia Vlachou, Giulia Stefenelli, Francesco Canonaco, Samuel Weber, Arjo Segers, et al.

Sources of particulate-matter air pollution and its oxidative potential in Europe

Kaspar R. Daellenbach[1,2,3], Gaëlle Uzu[4], Jianhui Jiang[1]✉, Laure-Estelle Cassagnes[1], Zaira Leni[5], Athanasia Vlachou[1], Giulia Stefenelli[1], Francesco Canonaco[1,6], Samuël Weber[4], Arjo Segers[7], Jeroen J. P. Kuenen[7], Martijn Schaap[7,8], Olivier Favez[9], Alexandre Albinet[9], Sebnem Aksoyoglu[1], Josef Dommen[1], Urs Baltensperger[1], Marianne Geiser[5], Imad El Haddad[1]✉, Jean-Luc Jaffrezo[4] & André S. H. Prévôt[1]✉

Particulate matter is a component of ambient air pollution that has been linked to millions of annual premature deaths globally[1–3]. Assessments of the chronic and acute effects of particulate matter on human health tend to be based on mass concentration, with particle size and composition also thought to play a part[4]. Oxidative potential has been suggested to be one of the many possible drivers of the acute health effects of particulate matter, but the link remains uncertain[5–8]. Studies investigating the particulate-matter components that manifest an oxidative activity have yielded conflicting results[7]. In consequence, there is still much to be learned about the sources of particulate matter that may control the oxidative potential concentration[7]. Here we use field observations and air-quality modelling to quantify the major primary and secondary sources of particulate matter and of oxidative potential in Europe. We find that secondary inorganic components, crustal material and secondary biogenic organic aerosols control the mass concentration of particulate matter. By contrast, oxidative potential concentration is associated mostly with anthropogenic sources, in particular with fine-mode secondary organic aerosols largely from residential biomass burning and coarse-mode metals from vehicular non-exhaust emissions. Our results suggest that mitigation strategies aimed at reducing the mass concentrations of particulate matter alone may not reduce the oxidative potential concentration. If the oxidative potential can be linked to major health impacts, it may be more effective to control specific sources of particulate matter rather than overall particulate mass.

Poor air quality associated with high levels of particulate matter (PM) is one of the five greatest health risks worldwide, alongside high blood pressure, smoking, diabetes and obesity[3,9]. Multiple factors are involved in the pathogenesis of non-communicable diseases resulting from exposure to PM. This makes causal links between health effects caused by PM and PM exposure and properties (composition, size) challenging to establish, especially for chronic effects of long-term exposures to low PM concentrations. One of the many pathways by which PM induces acute health effects is by causing an oxidant/anti-oxidant imbalance in the human respiratory system, which induces a cascade of inflammatory processes that increase the risks of cardiovascular and pulmonary diseases[10,11]. Accordingly, some epidemiological research has suggested that the oxidative potential (OP) of PM, which can be measured using acellular assays, would be a relevant metric for specific acute (not chronic) PM health effects[7,8]. As a result, considerable field and laboratory measurements have been devoted to the identification of PM components manifesting an oxidative activity, and the OP of these components is often related to the PM mass with which they are associated, OP^m (where OP^m is the OP activity per mass of the aerosol component, in units of nmol min^{-1} μg^{-1}) (refs. [7,12]). Focusing on different PM fractions, these studies have shown conflicting results[7], some pointing towards transition metals, for example, from primary vehicular emissions, as important drivers and others towards secondary organic aerosols (SOA). Often transition metals are not related to specific sources, nor are SOA precursors identified. Consequently, which emission sources of primary PM and SOA precursors control the OP concentrations (that is, OP^v, which is the OP activity per volume of air of the aerosol component, in units of nmol min^{-1} m^{-3}) and the exposure to OP of the population on a large scale remain unknown at present.

Here, we explore the sources of PM and OP across Europe, by combining field observations and air-quality modelling, and find that they are controlled by different sources. We use field observations to derive the OP^m parameters for the major European PM sources. For this, we have determined the chemical composition, sources and OP content of all PM

[1]Laboratory of Atmospheric Chemistry, Paul Scherrer Institute, Villigen, Switzerland. [2]Aix Marseille University, Centre National de la Recherche Scientifique (CNRS), Laboratoire Chimie Environnement (LCE), Marseille, France. [3]Institute for Atmospheric and Earth System Research/Physics, Faculty of Science, University of Helsinki, Helsinki, Finland. [4]Université Grenoble Alpes (UGA), Centre National de la Recherche Scientifique (CNRS), Institut de Recherche pour le Développement (IRD), Institute of Engineering and Management Univ. Grenoble Alpes (Grenoble INP), Institut des Géosciences de l'Environnement (IGE), Grenoble, France. [5]Institute of Anatomy, University of Bern, Bern, Switzerland. [6]Datalystica, Villigen, Switzerland. [7]Department of Climate, Air and Sustainability, The Netherlands Organisation for Applied Scientific Research (TNO), Utrecht, The Netherlands. [8]Institut für Meteorologie, Free University Berlin, Berlin, Germany. [9]Institut National de l'Environnement Industriel et des Risques (Ineris), Verneuil en Halatte, France. ✉e-mail: jianhui.jiang@psi.ch; imad.el-haddad@psi.ch; andre.prevot@psi.ch

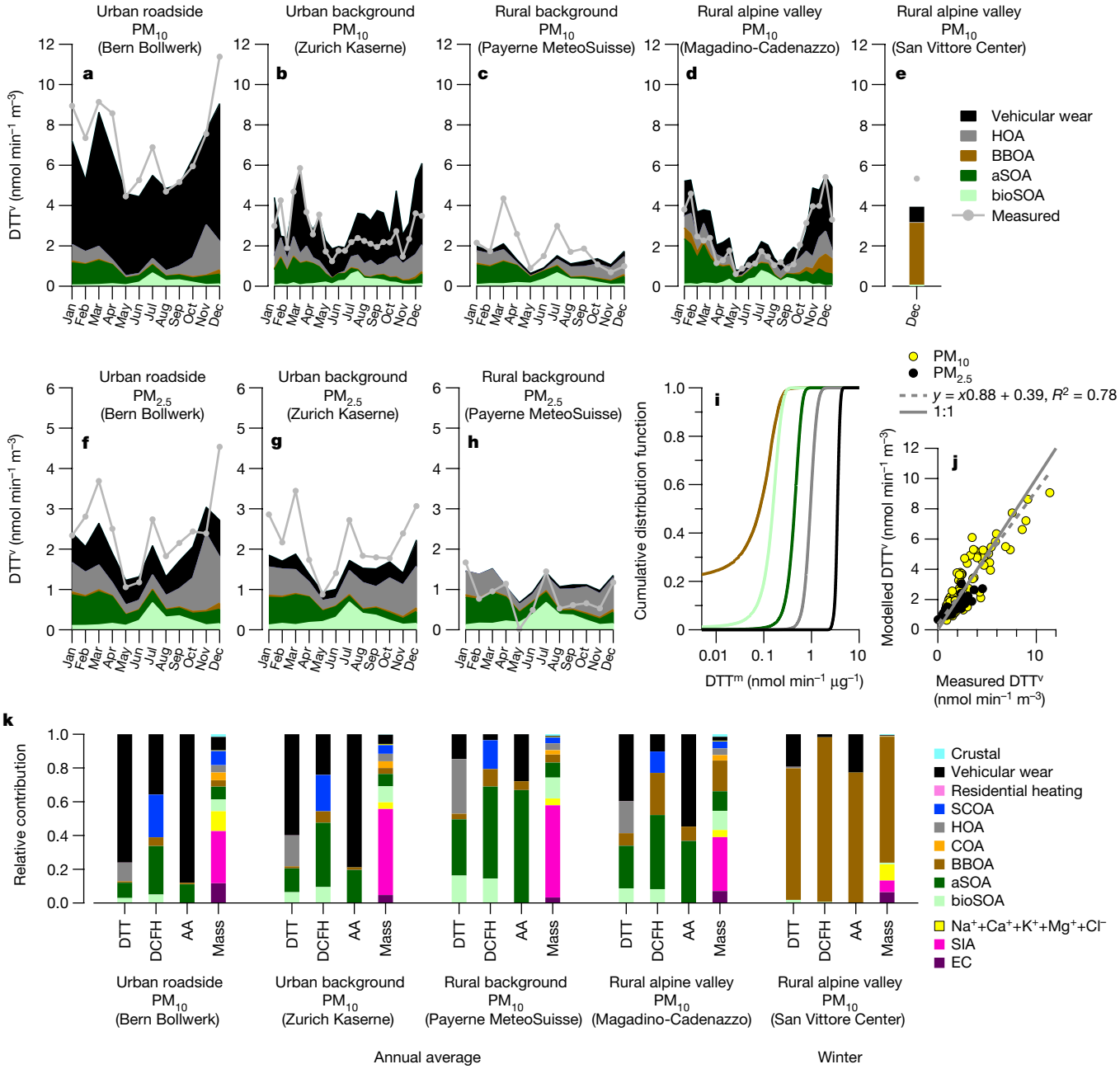

Fig. 1 | PM and OP^v sources at rural and urban sites. Contributions of metal (crustal, vehicular wear, residential heating) and OA (SCOA, HOA, COA, BBOA, aSOA, bioSOA) sources and other PM components to DTT^v_{PM10} and $DTT^v_{PM2.5}$ at five sites with different emission characteristics (109 composite samples) **a** and **f**, urban roadside; **b** and **g**, urban background; **c** and **h**, rural background; **d**, rural alpine valley; **e**, wintertime pollution episode in alpine valley; **i**, Cumulative distribution functions of DTT^m of contributing metal and OA sources; **j**, comparison between modelled and measured DTT^v; **k**, yearly (and winter for Alpine valley) average relative (concentration weighted) source contributions to DTT^v_{PM10}, $DCFH^v_{PM10}$, AA^v_{PM10} and PM_{10}. At the urban roadside, OP^v_{PM10} is dominated by non-exhaust vehicular emissions (61%–88%), mainly in the coarse mode. At the rural background site, anthropogenic SOA dominates OP^v_{PM10} (33%–67%). In alpine valleys, which are strongly affected by residential heating during winter, BBOA is more important for OP^v_{PM10} (7%–25%; 77%–97% during pollution events) than at the other sites (for example, rural background 3%–17%).

components (elements, and primary and secondary organic aerosol), using an extensive number of samples at sites where the major aerosol sources in Europe are present on a yearly basis (see Methods). Samples cover two size fractions: $PM_{2.5}$ and PM_{10}, referring to particles smaller than 2.5 µm and 10 µm, respectively. The OP^m parameters obtained were combined with a modified air-quality model to determine the main sources contributing to PM and OP exposure in Europe, where exposure refers to the amount of PM or OP^v in inhaled ambient air accumulated over a full year and integrated over the population.

We examined the contributions of different constituents to PM and their regional variability. PM mass concentration is dominated by regional secondary inorganic aerosol (SIA = NH_4^++NO_3^-+SO_4^{2-}, for PM_{10} 46 ± 13% and for $PM_{2.5}$ 56 ± 6%) (Fig. 1k), coming from the agriculture, transport and energy sectors. We quantified the sources of organic aerosol (OA) using a combination of offline aerosol mass spectrometry and positive matrix factorization[13,14]. In summer, OA is dominated by fine-mode secondary OA from biogenic precursors (bioSOA). The variation in bioSOA concentrations is consistent with (1) the exponential

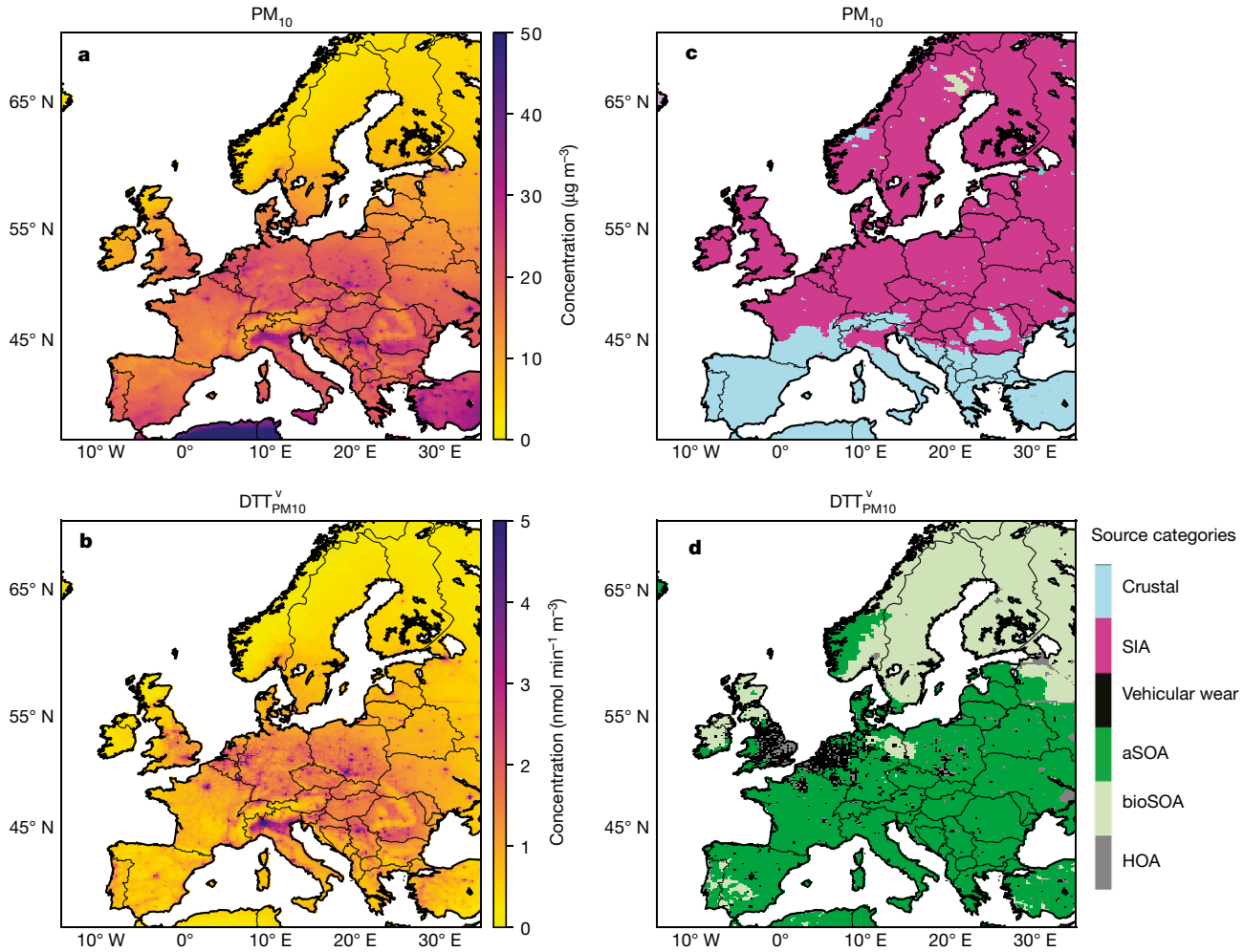

Fig. 2 | Levels and sources of PM10 and DTT$^{v}_{PM10}$ in Europe. OP^{v} and PM sources in Europe (only land surface displayed, spatial resolution: 0.25° × 0.125°) for the year 2011. **a**–**d**, Concentrations of PM_{10} (**a**) and DTT^{v}_{PM10} (**b**) are shown, as are sources dominating PM_{10} mass concentrations (**c**) and DTT^{v}_{PM10} (**d**), including crustal material (crustal), SIA (comprising $NH_4^+ + NO_3^- + SO_4^{2-}$), vehicular wear, anthropogenic SOA (aSOA), biogenic SOA (bioSOA), vehicular exhaust POA (HOA) (for other assays and $PM_{2.5}$, see Extended Data Fig. 5 and 7).

increase of biogenic terpene emissions with temperature[14], (2) the increased concentration of terpene oxidation products[15] (3-methyl-1,2,3-butanetricarboxylic acid (MBTCA) + pinic acid, Supplementary Fig. 4) and (3) the large contribution of non-fossil carbon during summer[16]. During winter, SOA is derived from the oxidation of anthropogenic precursors (aSOA, Extended Data Fig. 1, Supplementary Figs. 4 and 5), primarily from biomass burning[15]. aSOA strongly correlates with oxidation products of aromatic precursors arising from incomplete combustion (phthalic acid, polycyclic aromatic quinones, Extended Data Fig. 1, Supplementary Figs. 4 and 5) and lignin pyrolysis[15]. Unlike SOA, primary OA (POA) is more local (Supplementary Fig. 7) and is dominated by emissions from biomass burning during winter (BBOA), vehicles (HOA) and cooking (COA). Sulphur-containing OA (SCOA) probably derives from non-exhaust vehicular emissions, for example, tyre wear, because it correlates strongly with vehicular emissions (for example, NO_x), is composed of fossil carbon, and contributes mainly to the coarse mode of OA[14,16]. Finally, vehicular wear and crustal emissions dominate the coarse-mode metals, whereas in the fine mode, metals originate from residential heating (Supplementary Figs. 9, 10).

Since the particles that dominate PM mass concentration, with diameters of 0.1–5 µm, have a relatively constant probability of being deposited in the tracheobronchial region over this size range (Supplementary Fig. 28), both coarse PM and $PM_{2.5}$ should be considered when estimating the health effects of PM[17], as also suggested by the REVIHAAP project[18]. Therefore, we measured the OP^{v} related to $PM_{2.5}$ and PM_{10} using three different acellular assays (dithiothreitol (DTT), ascorbic acid (AA) and dichlorofluorescin (DCFH); see Methods section 'OP of PM'). Despite their variable sensitivity towards different aerosol constituents[19–21], DTT^{v} and AA^{v} correlate well with each other (correlation coefficient $R^2 = 0.68$) and to a lesser extent with DCFH^{v} (R^2(DTT^{v}, DCFH^{v}) = 0.35, R^2(AA^{v}, DCFH^{v}) = 0.45). We confirm for our case that exposing re-differentiated human bronchial epithelia to PM extracts with increasing DTT activity (16 biological experiments) enhances the release of the pro-inflammatory cytokine interleukin-6 (IL-6, Extended Data Fig. 2), triggering inflammation. Although the relevance of OP^{v} for the acute health risks of PM is still debatable[7,8], our results are in agreement with studies that suggest such links. Therefore, in the following we use OP^{v} as a representation of the acute health impacts of PM via pathological oxidative stress.

We quantified the OP^{m} (DTT^{m}, AA^{m}, DCFH^{m}) of the various OA and metal components based on a multiple linear regression model. We assessed the uncertainty of OP^{m} via Monte Carlo simulations (Fig. 1i, Methods section 'Sources of OP', Extended Data Figs. 3, 4). We note that we did not introduce any interaction term into the multiple linear regression model (Methods section 'Discussion of OP^{m} results'), although studies show that SIA, while not directly producing an OP

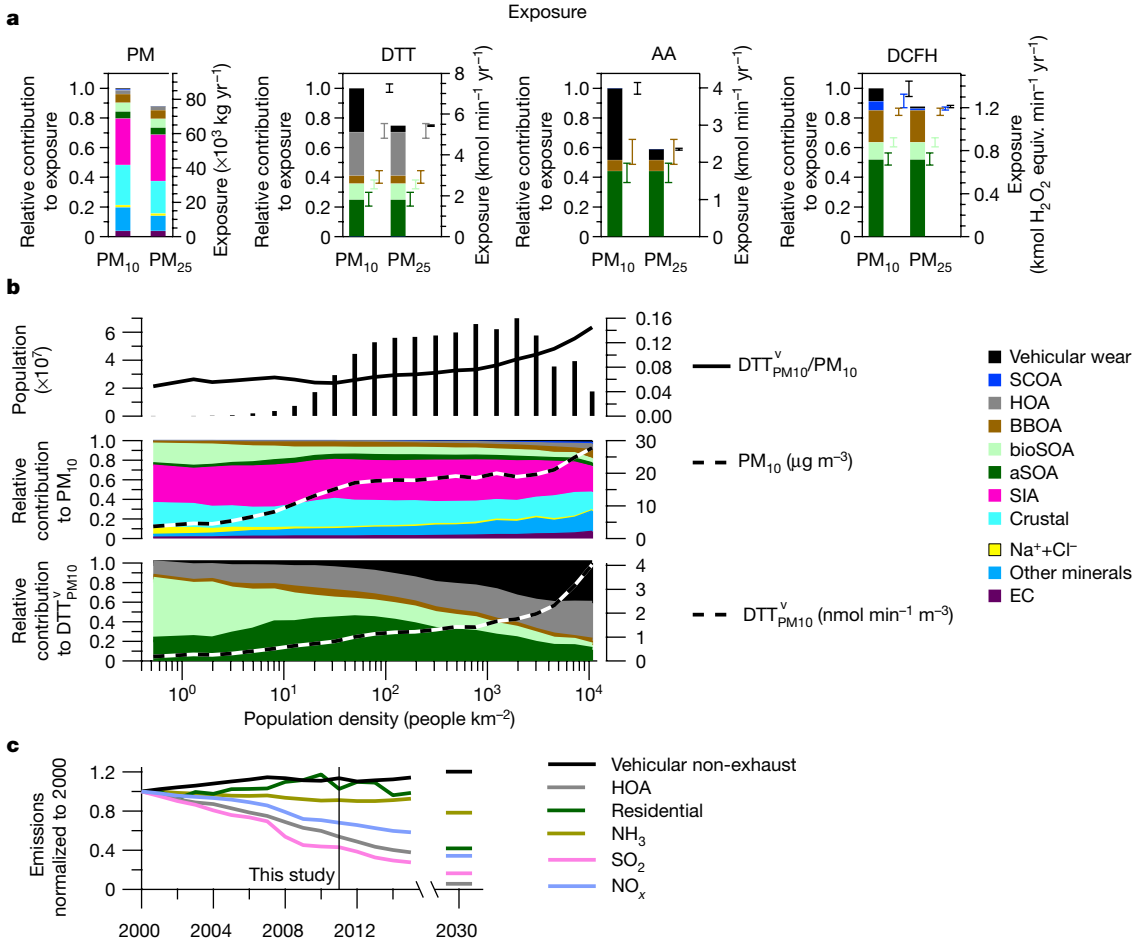

Fig. 3 | Source-segregated exposures to PM10 and OP^v_{PM10}, their dependence on population density, and historical and projected emissions. a, Contributions of aerosol sources and components to the total PM, DTT, DCFH and AA exposure for both PM_{10} and $PM_{2.5}$ in Europe (relative contribution to respective exposure and absolute exposure). Exposures are computed as population-integrated amount of OP^v or PM in inhaled ambient air accumulated over a full year. Error bars depict the range between the 25% and 75% quartiles obtained from the Monte Carlo analysis propagating the uncertainty of OP^m from the single sources from the multiple linear regression model. **b**, DTT^v_{PM10}/PM_{10} and population (top), PM_{10} concentrations and relative source contributions to PM_{10} (middle) and DTT^v_{PM10} and relative source contributions to DTT^v_{PM10} (bottom) in comparison to the population density in Europe. **c**, Past and projected anthropogenic emissions between 2000 and 2030 normalized to emissions from 2000 in Europe (the 28 European Union member countries plus Switzerland and Norway, with historical data from 2000–2015 and projections for 2030 based on the NEC Directive 2016/2284 targets; see Methods section 'Historical and projected emissions', Supplementary Figs. 29 and 30), PM_{10} vehicular exhaust emissions (HOA), PM_{10} vehicular non-exhaust emissions (which includes vehicular wear and SCOA), residential PM_{10}, mainly from heating emissions (similar to gas phase emissions, Supplementary Fig. 30), total NH_3, SO_2 and total NO_x emissions.

response (Supplementary Fig. 12), may facilitate metal dissolution, and thus inducing an indirect influence on OP[22].

We find that the OP based on the three different acellular assays responds to the same set of components (Fig. 1, Supplementary Table 2, Extended Data Figs. 3, 4). We demonstrate that anthropogenic emissions have a higher oxidative potential per mass unit of the aerosol component (OP^m) than biogenic emissions and crustal material. In the coarse mode, higher OP^m is found for non-exhaust vehicular emissions than for crustal material, which is in agreement with previous studies showing that transition metals have a large oxidative capacity[7]. The OP^m of aSOA, mainly from ageing of residential biomass burning emissions[15,16], is at least three times higher than the OP^m of bioSOA. This is in general agreement with laboratory experiments showing that SOA from single aromatic precursors have higher OP^m than biogenic terpene and isoprene SOA[7]. We note that potent reactive oxygen species, for example, quinones from the ageing of complex mixtures of polyaromatic hydrocarbons present in biomass smoke (Extended Data Fig. 1, Supplementary Fig. 6)[23], are enhanced during winter when aSOA dominates. Such species are often not accessible by ageing single precursors. This can explain the lower OP^m of laboratory SOA compared to ambient aerosol[7] (challenges in comparing OP^m between studies are described in Methods section 'Discussion of OP^m results'). Finally, we find different types of fine anthropogenic combustion POA (HOA, BBOA) to have a substantial OP^m, which agrees with earlier work[7]. Independent of the assay used, OP^v in the fine mode is largely explained by aSOA, with minor contributions from combustion derived POA and bioSOA (Fig. 1, Extended Data Fig. 3, 4). By contrast, OP^v in the coarse mode is mostly attributed to non-exhaust vehicular emissions (vehicular wear and SCOA), especially dominant at urban sites. These findings are in contrast with the source contributions to PM mass concentrations (Fig. 1), strongly affected by SIA. They also imply that reducing specific anthropogenic emissions will result in a considerable reduction of OP^v.

We combined the OP^m of the different sources with a modified air-quality model to predict the major sources of OP^v and PM mass concentrations in Europe (Fig. 2, Extended Data Fig. 5). The model reliably reproduces non-exhaust vehicular emissions, SIA, POA and SOA concentrations (Methods section 'Air-quality model')[24]. Modelled OP^v shows a good agreement with measured OP^v also for sites and

periods that were not included in the training dataset (Extended Data Fig. 6, Supplementary Fig. 26). This signifies that the model accurately represents the PM mass concentrations from various sources and supports the OP^m parameters derived from ambient observations. In Europe, OP^v and PM_{10} concentrations have hotspots in urban environments (for example, Paris and the Po valley), although PM_{10} concentrations are more regional than OP^v (Fig. 2a, b). Despite this, OP^v is dominated by different sources than is PM mass. PM mass is governed by regionally formed SIA in northern Europe and long-range transported crustal material in southern Europe (Fig. 2c, Extended Data Fig. 7). In contrast, DTT^v_{PM10} is dominated by anthropogenic SOA (largely from residential biomass burning) in large areas in Europe and vehicular emissions (non-exhaust and exhaust) in densely populated urban areas (Fig. 2d, Extended Data Fig. 7). As a result, PM mass concentrations are not only higher in urban areas (by a factor of about 7 compared to the area with the lowest population density), but urban PM has a threefold-higher OP per unit of PM mass concentration than rural PM (Fig. 3b, for $PM_{2.5}$ see Extended Data Fig. 8).

By scaling OP^v and PM mass concentrations with the population density, we estimate the contributions of different sources to OP and PM exposures. We find that modelled PM exposure (Fig. 3a, Extended Data Fig. 8) is governed by SIA (31%), crustal material (27%) and bioSOA (6%). The high contribution of SIA to PM exposure is consistent with the hypothesis that agricultural emissions drive PM-related premature mortality, as formulated by Lelieveld et al.[2]. By contrast, modelled OP exposure is overwhelmingly driven by anthropogenic sources (Fig. 3a), from non-exhaust vehicular emissions (15%–49%) in the coarse mode and aSOA (24%–51%) in the fine mode. It is worthwhile to note that aSOA could gain importance compared to PM from vehicular wear if aSOA, because of its size, is deposited in more vulnerable parts of the respiratory system. Observed differences between the sources of PM and OP exposures are much larger than the differences between the type of OP assay used or the uncertainties related to positive matrix factorization and the multiple linear regression model analyses (Fig. 3a, Supplementary Table 2). In densely populated regions, non-exhaust vehicular emissions dominate OP exposure, consistent with the increase in cardiovascular disease risk associated with highway proximity[25]. However, a large fraction of the population resides in less populated areas where the largest fraction of OP^v is ascribed to aSOA (Fig. 3b). As PM and OP exposures are governed by different sources, our finding could imply that acting on the dominant PM sources might not result in the anticipated reduction of the acute health effects of PM.

PM mass concentrations have substantially decreased in Europe[26] over the past decades (Supplementary Fig. 1), owing to efficient mitigation strategies that continuously reduced SIA precursors (SO_2, NO_x) and vehicular exhaust emissions[27] (Fig. 3c). However, the successful reduction of PM mass concentrations does not necessarily reflect a commensurate reduction in OP^v. In fact, the main sources of OP^v, including residential biomass burning (the main emitter of aSOA precursors) and non-exhaust vehicular emissions, have roughly remained constant over the past decades. With the increasing future demand for renewable energy for domestic heating, the eco-design directive (for example, the National Emission Ceilings (NEC) Directive 2016/2284[28], see Methods section 'Historical and projected emissions') has been recently implemented. Such implementation is expected to halve the residential emissions by 2030 (Fig. 3c, Supplementary Fig. 30), but only if cleaner combustion technologies are adopted. Otherwise, these emissions will remain stable for the next decade[29]. Although considerable efforts are still devoted to further reducing direct exhaust emissions, non-exhaust vehicular emissions are projected to slightly increase (Fig. 3c) with a future rise in vehicle numbers (for example, passenger car traffic volume increased by 27% in the 28 European Union member countries from 2010 to 2015[30,31]). With the phase-out of older vehicles with high PM exhaust emissions, non-exhaust emissions are expected to constitute 80%–90% of the direct road transport PM_{10} after 2020 (Supplementary Fig. 29)[27], unless additional measures are taken[17] (for example, reducing the copper content in brake pads, or a better sealing of the brakes). This could imply that targeting specific PM sources rather than overall PM mass might become more important for public health.

The aerosol sources examined here are widespread and can affect human health in other parts of the world. Further research is required to address other PM sources such as industrial metal emissions, heavy fuel oil combustion or coal emissions. The latter is a major PM source in highly populated urban environments in Asia, where most of the global PM-induced premature mortality is expected to occur. Our results show that different sources drive OP^v and PM mass concentrations, suggesting that knowing the sources of PM alone and taking action to reduce them is not sufficient to reduce the OP^v effectively. Although some studies have related OP^v to acute health effects such as acute cardiovascular and respiratory diseases, the main properties of PM that drive its chronic health effects, a leading cause of premature deaths, are yet to be determined and the role of OP^v in these effects remains undefined. If OP is found to be related to major health impacts this could imply that controlling its specific sources might be more effective. The framework developed here can be used to identify the sources responsible for the chronic health impacts of PM (for example, using long-term time series of PM components from different sources).

Online content

Any methods, additional references, Nature Research reporting summaries, source data, extended data, supplementary information, acknowledgements, peer review information; details of author contributions and competing interests; and statements of data and code availability are available at https://doi.org/10.1038/s41586-020-2902-8.

1. Apte, J. S., Marshall, J. D., Cohen, A. J. & Brauer, M. Addressing global mortality from ambient PM2. 5. *Environ. Sci. Technol.* **49**, 8057–8066 (2015).
2. Lelieveld, J., Evans, J. S., Fnais, M., Giannadaki, D. & Pozzer, A. The contribution of outdoor air pollution sources to premature mortality on a global scale. *Nature* **525**, 367–371 (2015).
3. Cohen, A. J. et al. Estimates and 25-year trends of the global burden of disease attributable to ambient air pollution: an analysis of data from the Global Burden of Diseases Study 2015. *Lancet* **389**, 1907–1918 (2017).
4. Valavanidis, A., Fiotakis, K. & Vlachogianni, T. Airborne particulate matter and human health: toxicological assessment and importance of size and composition of particles for oxidative damage and carcinogenic mechanisms. *J. Environ. Sci. Health C* **26**, 339–362 (2008).
5. Li, N., Hao, M., Phalen, R. F., Hinds, W. C. & Nel, A. E. Particulate air pollutants and asthma: a paradigm for the role of oxidative stress in PM-induced adverse health effects. *Clin. Immunol.* **109**, 250–265 (2003).
6. Xiao, G. G., Wang, M., Li, N., Loo, J. A. & Nel, A. E. Use of proteomics to demonstrate a hierarchical oxidative stress response to diesel exhaust particle chemicals in a macrophage cell line. *J. Biol. Chem.* **278**, 50781–50790 (2003).
7. Bates, J. T. et al. Review of acellular assays of ambient particulate matter oxidative potential: methods and relationships with composition, sources, and health effects. *Environ. Sci. Technol.* **53**, 4003–4019 (2019).
8. Weichenthal, S., Lavigne, E., Evans, G., Pollitt, K. & Burnett, R. T. Ambient PM 2.5 and risk of emergency room visits for myocardial infarction: impact of regional PM 2.5 oxidative potential: a case-crossover study. *J. Environ. Health* **15**, 46 (2016).
9. Forouzanfar, M. H. et al. Global, regional, and national comparative risk assessment of 79 behavioural, environmental and occupational, and metabolic risks or clusters of risks, 1990–2015: a systematic analysis for the Global Burden of Disease Study 2015. *Lancet* **388**, 1659–1724 (2016).
10. Crobeddu, B., Aragao-Santiago, L., Bui, L.-C., Boland, S. & Squiban, A. B. Oxidative potential of particulate matter 2.5 as predictive indicator of cellular stress. *Environ. Pollut.* **230**, 125–133 (2017).
11. Liu, Q. et al. Oxidative potential and inflammatory impacts of source apportioned ambient air pollution in Beijing. *Environ. Sci. Technol.* **48**, 12920–12929 (2014).
12. Shiraiwa, M. et al. Aerosol health effects from molecular to global scales. *Environ. Sci. Technol.* **51**, 13545–13567 (2017).
13. Daellenbach, K. R. et al. Characterization and source apportionment of organic aerosol using offline aerosol mass spectrometry. *Atmos. Meas. Tech.* **9**, 23–39 (2016).
14. Daellenbach, K. R. et al. Long-term chemical analysis and organic aerosol source apportionment at nine sites in central Europe: source identification and uncertainty assessment. *Atmos. Chem. Phys.* **17**, 13265–13282 (2017).
15. Daellenbach, K. R. et al. Impact of anthropogenic and biogenic sources on the seasonal variation of the molecular composition of urban organic aerosols: a field and laboratory study using ultra-high resolution mass spectrometry. *Atmos. Chem. Phys.* **19**, 5973–5991 (2019).

16. Vlachou, A. et al. Advanced source apportionment of carbonaceous aerosols by coupling offline AMS and radiocarbon size-segregated measurements over a nearly 2-year period. *Atmos. Chem. Phys.* **18**, 6187–6206 (2018).
17. Amato, F. et al. Urban air quality: the challenge of traffic non-exhaust emissions. *J. Hazard. Mater.* **275**, 31–36 (2014).
18. World Health Organization Regional Office for Europe. *Review Of Evidence On Health Aspects Of Air Pollution. REVIHAAP Project*. https://www.euro.who.int/en/health-topics/environment-and-health/air-quality/publications/2013/review-of-evidence-on-health-aspects-of-air-pollution-revihaap-project-final-technical-report (WHO, 2013).
19. Calas, A. et al. The importance of simulated lung fluid (SLF) extractions for a more relevant evaluation of the oxidative potential of particulate matter. *Sci. Rep.* **7**, 11617 (2017).
20. Charrier, J. & Anastasio, C. On dithiothreitol (DTT) as a measure of oxidative potential for ambient particles: evidence for the importance of soluble transition metals. *Atmos. Chem. Phys.* **12**, 9321–9333 (2012).
21. Sauvain, J.-J., Rossi, M. J. & Riediker, M. Comparison of three acellular tests for assessing the oxidation potential of nanomaterials. *Aerosol Sci. Technol.* **47**, 218–227 (2013).
22. Fang, T. et al. Highly acidic ambient particles, soluble metals, and oxidative potential: a link between sulfate and aerosol toxicity. *Environ. Sci. Technol.* **51**, 2611–2620 (2017).
23. Bruns, E. A. et al. Characterization of primary and secondary wood combustion products generated under different burner loads. *Atmos. Chem. Phys.* **15**, 2825–2841 (2015).
24. Jiang, J. et al. Sources of organic aerosols in Europe: a modeling study using CAMx with modified volatility basis set scheme. *Atmos. Chem. Phys.* **19**, 15247–15270 (2019).
25. Brugge, D., Durant, J. L. & Rioux, C. Near-highway pollutants in motor vehicle exhaust: a review of epidemiologic evidence of cardiac and pulmonary health risks. *J. Environ. Health* **6**, 23 (2007).
26. European Environment Agency *Air Quality In Europe 2016*. Report No. 28/2016, https://www.eea.europa.eu/publications/air-quality-in-europe-2016 (EEA, 2016).
27. Denier van der Gon, H. et al. Non-exhaust emissions. In *European Emission Inventories and Projections for Road Transport Non-Exhaust Emissions: Analysis of Consistency and Gaps in Emission Inventories from EU Member States* (ed. Amato, F.) Ch. 5, 101–121, https://www.sciencedirect.com/science/article/pii/B9780128117705000054 (Academic Press, 2018).
28. European Official Journal Directive (EU) 2016/2284 of the European Parliament and of the Council of 14 December 2016 on the reduction of national emissions of certain atmospheric pollutants, amending Directive 2003/35/EC and repealing Directive 2001/81/EC. https://eur-lex.europa.eu/legal-content/EN/TXT/?uri=uriserv%3AOJ.L_.2016.344.01.0001.01.ENG (2016).
29. Cofala, J. & Klimont, Z. *Emissions From Households And Other Small Combustion Sources And Their Reduction Potential*. TSAP Report 5, Version 1.0, https://ec.europa.eu/environment/air/pdf/TSAP-SMALL_SOURCES-20120612%5B1%5D.pdf (DG Environment of the European Commission, 2012).
30. European Environment Agency *Size Of The Vehicle Fleet*. https://www.eea.europa.eu/data-and-maps/indicators/size-of-the-vehicle-fleet/size-of-the-vehicle-fleet-8 (EEA, 2018).
31. European Statistical Office *Population And Population Statistics*. https://ec.europa.eu/eurostat/statistics-explained/index.php/Population_and_population_change_statistics (Eurostat, 2018).

Methods

Measurement sites

We collected 24-h integrated PM_{10} quartz-fibre filter samples every fourth day using a high-volume sampler (Digitel DHA-80, operated at 720 m^3 per 24 h) at nine sites in Switzerland and Liechtenstein subjected to different emission conditions during the entire year 2013 (Supplementary Table 1). For Bern (urban roadside), Zurich (urban background) and Payerne (rural background) we also collected $PM_{2.5}$ in 2013. Further, we collected PM_{10} and $PM_{2.5}$ in 2014 (Jan-Sep) with the same sampling strategy for Magadino (rural alpine valley). Additionally, we collected $PM_{2.5}$ and PM_{10} in a road tunnel (Islisbergtunnel on the Swiss highway A4, exit Wettswil am Albis, on a Tuesday, 20 May 2014, and a Sunday, 18 May 2014).

Analyses

Aerosol composition and gas-phase pollutants. We determined the bulk composition of OA with an aerosol mass spectrometer using filter samples following the procedures described in ref. [13]. This approach is composed of water-extracting the PM (milli-Q water, 18.2 MΩ cm, 30 °C, 20 min), followed by vortexing (60 s) and subsequent filtration using nylon membrane filters (pore size 0.45 µm, 8813Y-N-4, Infochroma AG). The resulting aqueous solutions were nebulized (custom designed APEX nebulizer, Elemental Scientific), dried (Nafion dryer) and measured by an Aerodyne high-resolution time-of-flight aerosol mass spectrometer, where sample analyses were alternating with analyses of milli-Q water and pure NH_4NO_3 solutions. The detailed working principles of the high-resolution time-of-flight aerosol mass spectrometer are summarized in Canagaratna et al.[32]. Data corrections were applied as outlined in Allan et al.[33] and Daellenbach et al. regarding the offline application of the aerosol mass spectrometer[13,14]. Field blanks were handled in the same way as exposed samples and showed a negligible signal.

We analysed 15 trace elements (Al, Fe, Ti, As, Cd, Cu, Mn, Mo, Ni, Pb, Rb, Sb, Se, V, Zn) by inductively coupled plasma mass spectrometry after acid digestion. Briefly, each sub-sample was acid-digested using HNO_3, and H_2O_2 in a microwave oven. Analysis took place with an inductively coupled plasma mass spectrometer (ELAN 6100 DRC II, Perkin Elmer)[34].

We measured 19 polyaromatic hydrocarbons: acenaphthene, fluorene, phenanthrene, anthracene, fluoranthene, 2-methylfluoranthene, pyrene, benzo[a]anthracene, chrysene, retene, benzo[e]pyrene, benzo[j]fluoranthene, benzo[b]fluoranthene, benzo[k]fluoranthene, benzo[a]pyrene, dibenzo[a,h]anthracene, benzo[g,h,i]perylene, indeno[1,2,3-cd]pyrene and coronene. Additionally, eight oxygenated-polyaromatic hydrocarbons (quinones) were measured: 1,4-naphthoquinone, 1,2-naphthoquinone, acenaphthenequinone, 9,10-anthraquinone, 1,4-anthraquinone, 2-methylanthraquinone, aceanthrenequinone and benz[a] anthracene-7,12-dione. The analyses were conducted using ultra-performance liquid chromatography/fluorescence (Thermo-Scientific, Dionex Ultimate 3000) and gas chromatography coupled to mass spectrometry with negative-ion chemical ionization (Agilent 7890A gas chromatograph coupled to 5975C mass spectrometer)[35–37] following a quick, easy, cheap, effective, rugged and safe (QuEChERS)-like extraction procedure of filter punches with acetonitrile as solvent[35,36]. Quality was assessed following the CEN (European Committee for Standardization) standard procedures EN 15549 and TS 16645 (2008 and 2014). In addition, the institute where the analyses were conducted (Institut National de l'Environnement Industriel et des Risques; Ineris) participates, every two years, in national and European polyaromatic hydrocarbon analytical inter-comparison exercises. The last exercise showed results in good agreement with reference values including the QuEChERS extraction[38]. Quinone extraction efficiencies were checked using NIST standard reference material (SRM 1649b, urban dust; https://www-s.nist.gov/srmors/view_cert.cfm?srm=1649B). Results obtained were in good agreement with NIST reference and indicative concentration values and with those previously reported in the literature[36].

We quantified anhydrous sugars (levoglucosan, galactosan and mannosan), sugar alcohols (xylitol, sorbitol, arabitol and mannitol) and glucose using high-performance liquid chromatography with the pulsed amperometric detector method[34,39]. Briefly, the water extract of a fraction of each sample was analysed on an ICS 5000+ high-performance liquid chromatograph with pulsed amperometric detection (Thermo-Fisher, equipped with a 4-mm-diameter Metrosep Carb 2 × 150-mm column and a 50-mm pre-column). The analytical run was isocratic with 15% of an eluent of sodium hydroxide (200 mM) and sodium acetate (4 mM) and 85% water, at 1 ml min^{-1}.

We quantified organic acids (glutaric, phthalic, methylglutaric, malonic, malic, pinic acids, and 3-3-methyl-1,2,3-butanetricarboxylic acid (MBTCA)) by liquid chromatography with mass spectrometry equipped with an electrospray ionization source (LCQ-Fleet, Thermo Fisher), with chromatographic separation performed on a Synergi 4-µm Fusion RP 80A column (Phenomenex), with a gradient of water–acetonitrile–formic acid eluent. The same water extract as for sugars and polyols was used for this analysis. Pinic acid and MBTCA are known oxidation products of biogenic terpenes[40]. Other organic acids are derived from anthropogenically dominated volatile organic compound emissions (for example, phthalic acid from naphthalene) or influenced by both biogenic and anthropogenic sources[40].

We quantified the organic and elemental carbon content by a thermo-optical transmission method using a Sunset OC/EC analyser (Sunset Laboratory Inc.)[41], following the EUSAAR-2 thermal-optical transmission protocol[42]. Major water-soluble ion concentrations (Na^+, Ca^{2+}, Mg^{2+}, SO_4^{2-}, NO_3^- and Cl^-) were measured using ion chromatography (Dionex ICS-3000 instrument)[43,44].

The gas-phase pollutants NO_x (chemiluminescence, Horiba APNA 360), SO_2 (ultraviolet fluorescence, CEN Norm EN 14212), CO (infrared absorption, CEN Norm 14212) and O_3 (ultraviolet absorption, Thermo Environmental Instruments 49C, Thermo Electron Corp.) and PM_{10} (gravimetric) were additionally monitored. The long-term variability of PM_{10} is displayed in Supplementary Fig. 1.

OP of PM. The oxidative potential of PM_{10} and $PM_{2.5}$ was assessed by extracting PM in simulated lung fluid and subsequent analysis by three different acellular assays (DTT, DCFH and AA), as described in detail in Calas et al.[19,45] and Foucaud et al.[46] (comparisons between DTT^v, AA^v, $DCFH^v$ and PM mass concentrations and PM components are shown in Supplementary Figs. 2 and 3).

Filters were extracted in a simulated lung fluid (here Gamble solution + dipalmitoylphosphateidylcholine) at 37 °C simulating the epithelial lung lining (extracellular environment) in the gas exchange region[19] during 1.25 h to take bioaccessibility with preferential solubility into account, and at iso-concentration of 25 µg ml^{-1} to get comparable results among different sites. PM extracts were not filtered after the extraction, and were submitted to the three OP assays in parallel. While DTT and AA are sensitive to redox-active PM constituents, DCFH reacts directly with oxidants in PM[7,47,48]. OP has been related to acute health outcomes (mostly from the DTT assay) and several studies have found a stronger association between OP and acute health effects than with PM[7].

The DTT assay is based on the ability of PM to transfer electrons from DTT to oxygen, generating a superoxide anion. We chose to use it here because it is the most frequently used approach owing to its relatively balanced response towards inorganic and organic atmospheric aerosol constituents[19,20,49]. The measurements were conducted according to the protocols in Calas et al.[45], adapted from Cho et al.[50].

The AA assay is based on the depletion of this natural lung antioxidant when in contact with PM. This assay can be used to quantify the transition-metal-based redox activities but has also shown to be sensitive to (organic) biomass burning tracers[21,45]. The AA assay is modified from Mudway et al.[51] and is fully described in Calas et al.[45]

The DCFH assay relies on a non-fluorescent probe, which is oxidized to a fluorescent product in the presence of reactive oxygen species and horseradish peroxidase. This assay is usually used in biology to detect reactive oxygen species at cellular level and has been adapted for acellular assays[46]. This probe is known to be non-specific to oxidant species[51,52], but also to reactive nitrogen species. The procedure relies on Foucaud et al.[46].

Analysis of biological response. The inflammatory response of normal human bronchial epithelial cells to exposure of PM from the urban roadside (Bern-Bollwerk) and the rural valley site (Magadino-Cadenazzo) was assessed in different seasons. For this purpose, the PM filter samples (exposed diameter of 14.7 cm) were pooled to form seasonal composites (each sample represented by a circular punch of 10 mm diameter, 0.8 cm^2), that is, January to March (Bern winter 2013 PM_{10}, Bern winter 2013 $PM_{2.5}$, Magadino winter 2013 PM_{10}, Magadino winter 2014 PM_{10}) and July to August (Bern summer 2013 PM_{10}, Bern summer 2013 $PM_{2.5}$, Magadino summer 2013 PM_{10}, Magadino summer 2014 PM_{10}). Immediately before the cellular exposure, the composites were extracted in 7 ml milli-Q water (milli-Q water, 18.2 MΩ cm, 30 °C), homogenized by vortexing (1 min) and filtered through a 0.45-µm nylon membrane syringe filter (Infochroma AG, Zug, Switzerland). Field blanks were extracted with the same procedure using an equivalent filter surface area as for the samples.

Human bronchial epithelial cells were isolated from human donor lungs. Two normal lung samples deemed not suitable for transplantation were obtained from the Life Alliance Organ Recovery Agency of the University of Miami, USA. Institutional-Review-Board-approved consent for research with these tissues was obtained by the Life Alliance Organ Recovery Agency and conformed to the Declaration of Helsinki. Air–liquid interface cultures of re-differentiated human bronchial epithelial cells were generated as previously described[53]. Cell cultures were exposed to PM extracts for 4 h (7.4–22.2 µg per cm^2 of cell culture area and 1:10 diluted resulting in 0.7–2.2 µg per cm^2 of cell culture). Control cell cultures were either exposed to extracts from field blanks or left untreated in the incubator. Repeatability was assessed by performing 3–9 experiments for each seasonal composite. The release of the inflammatory mediator IL-6 was measured in the basolateral compartment collected at 24 h after exposure to filter extracts, using the Bio-Plex multiplex bead-based suspension array system and the appropriate detection kit (Bio-Rad Laboratories AG) according to the manufacturer's protocol.

Source apportionment of OA and trace elements

Positive matrix factorization. We performed source apportionment of the OA and of trace metals using positive matrix factorization, which is a statistical unmixing model[54]. Positive matrix factorization explains the variability in a chosen dataset ($x_{i,j}$) with linear combinations of constant factor profiles ($f_{k,j}$) representing the chemical composition of the sources/components) and their contribution varying in time and/or space ($g_{i,k}$). Since positive matrix factorization allows only for positive results ($g_{i,k}$,$f_{k,j}$), it is ideal for environmental purposes. The residual is termed $e_{i,j}$. The index i represents a measurement (time and space), j an observed variable (trace metal, ion in aerosol mass spectrometer), and k is a factor.

$$x_{i,j} = \sum_{k=1}^{p} g_{i,k} f_{k,j} + e_{i,j} \quad (1)$$

This equation is solved by Multilinear Engine 2 (ref. [55]) and controlled by the software Source Finder (SoFi[56]).

Sources of OA. Multilinear Engine 2 allows using a priori information by constraining known factor profiles $g_{i,k}$ within a certain range defined by the scalar a value ($0 \le a \le 1$).

$$f_{k,j} = f'_{k,j} \pm a f'_{k,j} \quad (2)$$

For the source apportionment of the OA in PM_{10} at the nine sites in Switzerland and Liechtenstein during 2013 (see Daellenbach et al.[14]), we used reference spectra representing HOA and COA (Crippa et al.[57]). The sources' contributions to water-soluble OA were subsequently corrected to contributions to OA using source-specific recoveries derived in Daellenbach et al.[13] and confirmed in other studies[16,58]. The evaluation, sensitivity tests (a-value, extreme bootstrap scenarios, source-specific recoveries) and uncertainty estimates of the organic source apportionment results were presented in Daellenbach et al.[14]. For Magadino (2013 and 2014), an analogous separate size-resolved ($PM_{2.5}$ and PM_{10}) source apportionment analysis (HOA constrained from Crippa et al.[57]) was performed and presented in Vlachou et al.[16]. The time series of the resolved OA source contributions are compared to other chemical analyses in Supplementary Fig. 4. aSOA time series are compared to phthalic acid and quinone concentrations (Extended Data Fig. 1, Supplementary Fig. 5) and bioSOA to MBTCA concentrations (Extended Data Fig. 1, Supplementary Fig. 5). In Extended Data Fig. 1 (Supplementary Fig. 6), the relative contribution of quinones to OA is presented.

Sources of trace metals. We performed unconstrained (no a priori knowledge) positive matrix factorization using trace metal data (Al, As, Cd, Cu, Fe, Mn, Mo, Ni, Pb, Rb, Sb, Se, Ti, V and Zn). We used PM_{10} and $PM_{2.5}$ samples including samples from an urban roadside site (Bern, Bollwerk, 24 samples), an urban background site (Zurich, Kaserne, 36 samples), Magadino (rural site affected by wood burning, 58 samples), S. Vittore (wintertime wood-burning pollution episode at rural site, 1 sample) a rural background site (Payerne, MeteoSuisse, 24 samples) and a road tunnel (4 samples).

The data matrix $x_{i,j}$ consists of the concentrations determined for the mentioned trace metals (if the concentration was smaller than the half the quantification limit, QL/2). The error matrix $s_{i,j}$ was computed using the quantification limit and a term depending on the concentration.

$$s_{i,j} = \sqrt{(\mathrm{QL}_j)^2 + (\sqrt{x_{i,j}})^2} = \sqrt{(\mathrm{QL}_j)^2 + x_{i,j}} \quad (3)$$

As an overall measure of the quality of the data representation, we used Q/Q_{exp} (where $Q = \sum_{i,j} \frac{(e_{i,j})^2}{(s_{i,j})^2}$ and $Q = nm - p(n+m)$, where n and m are the number of samples and the number of variables). Q/Q_{exp} was small (around 1) when employing only one or two factors, which could indicate that the uncertainty $s_{i,j}$ was overestimated (Supplementary Fig. 8). A clear seasonality in the uncertainty-weighted residuals $e_{i,j}/s_{i,j}$ was observed for the two-factor solution (higher in winter than summer; Supplementary Fig. 8). When employing three factors, there was no longer any apparent seasonality in $e_{i,j}/s_{i,j}$ and Pb and Zn were better explained by the factorization (Supplementary Fig. 8). The three-factor separation is displayed in Supplementary Figs. 9 and 10, yielding:

(1) a component perceived mostly in the coarse mode of PM explaining Al, Se and Ti contents and thus identified as crustal material.

(2) another component also perceived mostly in the coarse mode of PM, but explaining Cu, Fe, Mo and Sb contents, which—in contrast to crustal material—were also strongly enhanced in a road traffic tunnel. This component was therefore related to vehicular wear[59].

(3) a third component explaining Cd, Pb, Rb and Zn contents. This component was perceived mostly in $PM_{2.5}$ and showed a temporal behaviour similar to combustion-related components (enhanced in winter compared to summer). Thus, this component was identified as emissions from residential heating.

We performed 100 bootstrap runs (including/excluding samples and initializing model information randomly to assess the rotational ambiguity) to obtain robust source contributions and to estimate the uncertainty related to fingerprints (chemical composition) and time series. The chemical fingerprints (and uncertainties) of the separated sources are presented in Supplementary Fig. 9 and the concentration time series in Supplementary Fig. 10 (uncertainty in Supplementary Fig. 11). While

vehicular wear and crustal material had a relatively small uncertainty, residential heating was found to be more uncertain (Supplementary Fig. 11). The time series of the resolved metal source contributions is compared to the other chemical analyses in Supplementary Fig. 4.

Size distribution of source concentrations. Five of six OA sources were mostly present in $PM_{2.5}$, whereas SCOA represented coarse fossil organic material related to traffic activity (NO_x)[14,16]: $HOA(PM_{2.5}) = HOA(PM_{10}) \times 0.7 + 0.17$, $COA(PM_{2.5}) = COA(PM_{10}) \times 0.7 + 0.17$ (based on the assumption that COA shows the same behaviour as HOA), $BBOA(PM_{2.5}) = BBOA(PM_{10}) \times 0.70 + 0.08$, $SCOA(PM_{2.5}) = SCOA(PM_{10}) \times 0.15 + 0.05$, $aSOA(PM_{2.5}) = aSOA(PM_{10}) \times 0.66 + 0.09$, $bioSOA(PM_{2.5}) = bioSOA(PM_{10}) \times 0.96 + 0.30$. From the size-resolved source apportionment analysis, vehicular wear was found to be mostly present in PM_{10} ($PM_{2.5} = PM_{10} \times 0.15$).

Sources of OP

Multiple linear regression model. To explain the spatial and temporal variability of OP^v, both land-use regression and source impact regression models were used in previous studies (here we cite only a selection)[7,12,60–64]. In this study, we used a source impact regression model to derive OP^m and source contributions to OP^v. OP^v was apportioned to its sources using a multiple linear regression model as in equation (4). OP^v (in units of nmol min^{-1} m^{-3}) and OP^m (in units of nmol min^{-1} μg^{-1}) are the OP activity per volume of air and per mass of the respective aerosol component *i*. OA source concentrations are termed OA_i (in units of $\mu g\ m^{-3}$) and metal source concentrations MA_i (in units of $\mu g\ m^{-3}$) (the sources' time series are compared to OP^v in Supplementary Fig. 3).

$$OP^v(t) = \sum_i OP^m_{OA_i} \times OA_i(t) + \sum_i OP^m_{metal_i} \times MA_i(t) \quad (4)$$

This equation was fitted as a least-squares regression without constraints. Overfitting was prevented by forward selection of predictors based on the Akaike information criterion (AIC, *k* being the number of predictors used in the regression, RSS being the squared sum of squares, *n* being the number of points used in the regression, and OP^v_{meas} and OP^v_{mod} being the measured and modelled OP).

$$AIC = 2k - n \ln\left(\frac{\sum_t (OP^v_{meas}(t) - OP^v_{mod}(t))^2}{n}\right) = 2k - n \ln\left(\frac{RSS}{n}\right) \quad (5)$$

We used 109 samples: 24 from an urban roadside site (Bern, Bollwerk), 36 from an urban background site (Zurich, Kaserne), 24 from a rural background site (Payerne, MeteoSuisse), 24 from a rural background site in an alpine valley affected by wood burning (Magadino-Cadenazzo), and one from a wintertime wood-burning pollution episode in an alpine valley (San Vittore). Possible candidate predictors considered were trace-metal sources (crustal material, vehicular wear, residential heating) and OA sources (HOA, COA, BBOA, SCOA, aSOA, bioSOA). Whereas the majority of OA sources were mostly present in $PM_{2.5}$, SCOA represented coarse fossil organic material (see Methods section 'Size distribution') related to traffic activity (NO_x)[14,16]. We used the known size distribution ($PM_{2.5}$ versus PM_{10}) for estimating the OA sources in $PM_{2.5}$ based on the source concentrations in PM_{10}. For the metal sources, we used the directly measured distribution from the source apportionment analysis. NH_4NO_3 and $(NH_4)_2SO_4$ were excluded, since—in agreement with literature[45,47]—these components did not induce OP (Supplementary Fig. 12). Elemental carbon was excluded because it is influenced by several combustion sources (traffic, biomass burning).

For DTT, a model with five predictors had the lowest AIC (Supplementary Fig. 13). Whereas models with six predictors had a comparable AIC, the Bayesian information criterion (a stronger penalty term for including more predictors than AIC) suggested that the five-predictor models were clearly favourable. Of the five-predictor models, there were two of similar quality (vehicular wear, HOA, BBOA, aSOA and either bioSOA or COA). Since $PM_{2.5}$ DTT^v as well as PM_{10} DTT^v showed an increase in summer, suggesting the importance of bioSOA, we chose the model with bioSOA. Using AIC as the decisive metric, we also chose for DCFH a five-predictor model with vehicular wear, SCOA, BBOA, aSOA, and bioSOA (Supplementary Fig. 14). For AA, a 3-predictor model using vehicular wear, BBOA, and aSOA was chosen, since including further predictors did not lead to further improvement using the AIC as metric (Supplementary Fig. 15).

The multiple linear regression model uncertainty and the sensitivity of OP^m (DTT^m, AA^m, $DCFH^m$) to errors in OP^v measurements and PM source apportionment were assessed via Monte Carlo simulations (50,000 runs). In this process, we combined different randomly selected OA and metal source apportionment solutions, and additionally performed bootstrap analysis on the time points (cumulative density functions of OP^m (Fig. 1, Extended Data Figs. 3, 4, Supplementary Table 2).

Discussion of OP^m results. Transition metals have been shown to have a substantial impact on the OP activity of PM[20,21,65–69]. In this study, we find that vehicular wear induces a strong impact on OP. Overall, this is consistent with findings from London suggesting that coarse traffic emissions have a higher OP^m than PM from other sources[64].

Aqueous solutions of NH_4NO_3 (0.08–40.02 $\mu g\ ml^{-1}$) and $(NH_4)_2SO_4$ (0.13–66.07 $\mu g\ ml^{-1}$) were analysed with the DTT and AA assays and did not exhibit reactivity (Supplementary Fig. 12, analyses of ambient PM conducted at 25 $\mu g\ ml^{-1}$). This is in agreement with literature[45] and previously reported results for DCFH[47]. We note that we did not introduce any interaction term into the multiple linear regression model, although studies show that SIA, while not directly inducing an OP response, can facilitate the metal dissolution, having an indirect influence on OP[22]. We observe such nonlinear matrix effects when using OP^m parameters derived from the multiple linear regression model in a road tunnel where vehicular wear is dominant: OP^v from vehicular wear alone overestimated the measured OP^v (DTT^v: 3×, AA^v: 2×, $DCFH^v$: 3×) as SIA is minimal and thus metals are not soluble. However, the multiple linear regression model explains the OP^v measurements well (Fig. 1, Extended Data Figs. 3, 4) and thus such effects apparently have a minor role under ambient conditions.

Earlier studies showed that both POA and SOA have a substantial impact on OP^v (refs. [7,62,69–77]). We find that aSOA has a higher OP^m than bioSOA. This is in agreement with literature showing that the SOA precursor type has a strong impact on OP^m. SOA from anthropogenic aromatic precursors (for example, naphthalene and phenanthrene) has a higher OP^m than SOA from biogenic precursors (for example, α-pinene, isoprene and limonene)[72,73,78,79]. This is consistent with previous research pointing out the important role of quinones formed from aromatic compounds on OP^v (refs. [50,80,81]). Further, also different types of fine anthropogenic combustion POA (HOA and BBOA) were found to have a considerable OP^m, which is in agreement with earlier work[70,71,82].

Quantitative comparisons of $OP^{m,PM}$ (here reported in units of nmol min^{-1} per µg of $PM_{2.5}$; but elsewhere in this paper OP^m is consistently reported in units of nmol min^{-1} per µg of source mass) between measurement techniques remain challenging because of differences in measurement techniques as stated by Bates et al.[7]. Nevertheless, we compare the measured $OP^{m,PM}$ value that we find for $PM_{2.5}$ (as is usually reported in the literature) to the results in this study. $OP^{m,PM2.5}$ values in this study (an annual average for measurement sites between 60 and 140 nmol min^{-1} per µg of $PM_{2.5}$) are at the upper end of ambient $OP^{m,PM}$ values previously reported (between 10 and 80 nmol min^{-1} per µg of $PM_{2.5}$)[12].

Air-quality model

Modelling PM contribution in Europe. We used the regional chemical transport model Comprehensive Air Quality Model with extensions (CAMx) version 6.3 (http://www.camx.com) to simulate air quality in Europe in 2011 (Supplementary Fig. 16), with a spatial resolution of 0.25° × 0.125° and 14 terrain-following vertical layers, with the first layer being about 20 m thick. The meteorological parameters

were calculated using the Weather Research and Forecasting Model WRF-ARW version 3.7.1 (ref. [104]) The Carbon Bond 6 Revision 2 (CB6r2) mechanism[83] was used for gas-phase chemistry. Partitioning of inorganic aerosol components (sulphate, nitrate, ammonium, sodium and chloride) between the gas and particle phases was calculated by the ISORROPIA thermodynamic model[84]. OA formation was estimated by the 1.5-dimensional volatility basis set OA chemistry/partitioning module[85]. The volatility basis set module of the model was modified to separate the contributions of specific OA sources including biomass burning, gasoline and diesel vehicles, other anthropogenic activities and biogenic sources[86,87]. The parametrization of biomass burning and vehicles was updated based on Ciarelli et al.[86] and Platt et al.[88], respectively. The source-specific anthropogenic emissions were obtained from the high-resolution European emission inventory TNO-MACC-III (The Netherlands Organization for Applied Scientific Research—Monitoring Atmospheric Composition and Climate)[89]. Biogenic emissions were prepared using the PSI model[87]. The initial and boundary conditions were obtained from the MOZART (Model of Ozone and Related Chemical Tracers) global model datasets MOZART-4/ GEOS-5, which are widely used in chemical transport models. The MOZART-4 data divided dust into four size bins ranging from 0.05 μm to 5.0 μm, and with the largest contribution found in dust bin 2 (0.5–1.25 μm)[90–92]. The modelled gas and aerosol concentrations (OA separated into different POA and SOA categories, NH_4^+, NO_3^-, SO_4^{2-} and elemental carbon) were in good agreement with data from the European air-quality database AirBase v7 and measurements from Aerodyne aerosol chemical speciation monitor or Aerodyne aerosol mass spectrometer stations[24,86,87]. The modelled OA components were reclassified into four categories to match the source apportionment of OP: (1) HOA: the sum of POA from vehicles and from other fossil fuel combustion emissions; (2) BBOA: the POA from biomass burning (and other residential heating sources such as coal); (3) bioSOA: the SOA from biogenic emissions; and (4) aSOA: the sum of SOA from all anthropogenic sources (Supplementary Fig. 16). The species related to non-tailpipe emissions of traffic such as metals from vehicular wear and SCOA were not explicitly represented in the model. In addition, the emission information on these components is highly uncertain and emission factors vary largely from country to country. As the emissions of vehicular wear and SCOA originate from the road traffic and show high correlation with the traffic-NO_x emissions, we estimated the levels of vehicular wear and SCOA as functions of NO_x from vehicles (Supplementary Fig. 17). The size distributions of vehicular wear and SCOA were computed based on a parametrization derived from the measurements (Supplementary Fig. 18). As the model simulates total NO_x from all sources, we calculated the NO_x from road traffic by multiplying the total NO_x with the grid-scale ratio of NO_x emissions from road traffic to total NO_x emissions (Supplementary Fig. 19). The estimated copper concentration from vehicular wear (copper being 4.5% of total vehicular wear as found by metal positive matrix factorization) agreed well (absolute concentrations and spatial distribution) with PM_{10} copper concentrations from brake wear modelled independently (analogously to Hulskotte et al.[93]) (Supplementary Fig. 20). Additionally, total measured copper concentrations from different European sites agreed with the estimated copper concentrations from vehicular wear (data from EBAS; http://ebas.nilu.no/) quite well (Supplementary Figs. 20–22)[94,95]. However, at some sites local point sources (not vehicular wear) result in total measured copper concentrations much higher than the modelled vehicular wear copper concentrations.

Modelling OP^v contribution in Europe. OP^v (DTT^v, $DCFH^v$, AA^v) were modelled using the parameterization from the field data. To estimate the spatial distributions of OP^v (DTT^v, $DCFH^v$ and AA^v) in Europe, the median values of OP^m of all sources were multiplied with the modelled concentrations of the relevant OA components (HOA, BBOA, bioSOA, aSOA and SCOA) and vehicle wear metal. The modelled DTT^v, AA^v and $DCFH^v$ from the relevant sources are presented in Extended Data Fig. 5 and the most important sources for DTT^v, AA^v, $DCFH^v$ and PM concentrations are displayed in Extended Data Fig. 7.

A Monte Carlo approach with 300 runs for each OP assay was conducted to assess the uncertainties of the estimated OP^v. Three sources of uncertainty were included: (1) OP^m of each assay; (2) parametrization of SCOA and vehicle wear as a function of road traffic NO_x; and (3) parametrization of the size distributions of SCOA and vehicular wear ($PM_{2.5}$ versus PM_{10}). We note that (1) includes both uncertainties related to the positive matrix factorization analysis and the multiple linear regression model parameterization. For each run, a set of OP^m combinations was randomly selected among OP^m combinations generated by the multiple linear regression model developed in this study. A comparison between all and selected OP^m combinations shown in Supplementary Fig. 23 indicates that the distribution of OP^m was well represented by the randomly selected values. The factors (2) and (3) were sampled from the normal distributions with the mean value and standard error shown in Supplementary Figs. 17 and 18.

Model validation. An accurate representation of PM OP in Europe based on our measurements entails two major requirements: (1) PM sources at our sites must be representative of sources encountered in Europe; and (2) OP^m determined from our measurements for the different sources are consistent across Europe and not highly dependent on the emission conditions. Below, we demonstrate that these two requirements are fulfilled in our analysis:(1) The sources contributing to PM found at our measurement sites are identified as the major and most widespread sources throughout Europe, and the PM chemical composition is consistent overall with other European sites[96,97]. The OA components extracted by positive matrix factorization (HOA, BBOA, aSOA and bioSOA) are very frequently reported at other sites and the modelled population-weighted concentrations in Europe compare well with the measurements at the Swiss sites investigated here (Supplementary Fig. 24). We are aware that we cannot represent coal combustion (though included as a part of biomass burning), which is important in Poland, or local industrial emissions, as pointed out in the main text. Assessing the impact of local sources requires city-level modelling, and coal combustion should be targeted in future research, especially in the context of China.(2) The OP^m for a specific source is a property of the chemical composition of the aerosol emitted by this source. The chemical fingerprints of the sources found in this study are similar to those reported at other European sites[96,98]. We compare OP^m estimated here for vehicular wear and primary biomass burning with estimates made at two sites in France dominated by these sources (Alpine Valley site for biomass burning and traffic site for vehicular wear, Supplementary Fig. 25)[45]. Results from France are largely in agreement with our results from the multiple linear regression (MLR) at least for these two sources (for DTT, the median values are: OP^m(BBOA(MLR)) = 0.08 nmol min^{-1} per μg of source mass versus OP^m(BBOA(France)) = 0.22 nmol min^{-1} per μg of source mass; OP^m(vehicular wear(MLR)) = 3.51 nmol min^{-1} per μg of source mass versus OP^m(vehicular wear(France)) = 1.40 nmol min^{-1} per μg of source mass). We also compare the modelled OP^v to measurements from 2011 that were not part of the training dataset. We use samples from Zurich (Switzerland, 19 samples) and from an additional site in Lens[34], France (95 samples, Extended Data Fig. 6). All the predicted OP assays show remarkable agreement with the measurements (Supplementary Fig. 26), with R values of 0.83, 0.71, 0.67 for DTT^v, AA^v and $DCFH^v$, respectively. The model accurately captures DTT^v (−13%) and AA^v (5%), whereas $DCFH^v$ is underestimated by 40%, as assessed by the median relative difference between model and measured OP^v $\left(\text{median}\left(\frac{OP^v_{mod} - OP^v_{meas}}{OP^v_{meas}}\right)\right)$. This signifies (1) that the model accurately represents the PM mass concentrations from the various sources and (2) that the OP^m values determined for the various sources based on the parameterization of ambient observations are applicable to both sites. Taken together, these comparisons highlight the accuracy of

our model in predicting PM mass and the representativeness of our parameterizations for Europe.

Inhalation exposure of PM and OP

We compute the PM and OP exposure as the population integrated amount in inhaled ambient air accumulated over a full year (Supplementary Fig. 27). In essence, exposure is proportional to the product of OP or PM concentration and population density. The exposure to PM and OP for one individual *i* in age group *j* was estimated based on equation (7):

$$E_{i,j} = C_{\text{air}} \times \text{IR} \times \text{ET} \times \text{EF} \quad (7)$$

where C_{air} ($\mu g\ m^{-3}$) is the concentration of the PM component or OP (nmol $min^{-1}\ m^{-3}$ or nmol of $H_2O_2\ min^{-1}\ m^{-3}$) in the air, IR is the inhalation rate ($m^3\ h^{-1}$), ET is the exposure time, which we assumed to be 24 h per day, and EF is the exposure frequency, which we assumed to be 365 days. The inhalation rate for each age group was compiled based on the European Chemicals Agency[99] for age <30 years and the US Environmental Protection Agency[100] for age >30 years (presented in Supplementary Table 3). PM and OP exposure on the regional scale were then calculated by summing up the exposure of all individuals *i* in all age groups *j*.

$$E = \sum_j \sum_i E_{i,j} \quad (8)$$

Multiple-Path Particle Dosimetry Model

We used the Multiple-Path Particle Dosimetry Model (MPPD)[101] to estimate the number of particles deposited in the human body in comparison to the number of inhaled particles, termed deposited fraction (pulmonary and tracheobronchial region) (Supplementary Fig. 28).

Historical and projected emissions

Historical emissions in Europe (the 28 European Union member countries plus Switzerland and Norway) from 2000–2015 are obtained from the Copernicus Atmosphere Monitoring Service (CAMS) regional emission inventory (a further development of the TNO-MACC inventory), which was based largely on the emissions reported by countries under the NEC Directive 2016/2284[28] and the Convention on Long-Range Transboundary Air Pollution[89]. This includes direct PM_{10} emissions from traffic exhaust emissions (HOA), PM_{10} traffic non-exhaust emissions (vehicular wear), PM_{10} residential emissions, mainly from heating (including gas-phase emissions; Supplementary Fig. 30), and gas-phase emissions of total SO_2 and total NO_x. Projected emissions for 2030 are estimates, assuming that the targets in the NEC Directive 2016/2284[28] are met. The sectoral emissions under these scenarios were obtained from the GAINS (Greenhouse Gas–Air Pollution Interactions and Synergies) model hosted by the International Institute of Applied Systems Analysis (IIASA) in Laxenburg (Austria)[102]. These results are presented in Fig. 3c, and in addition, a more detailed comparison of the historical exhaust and non-exhaust road traffic emissions is presented in Supplementary Fig. 29.

Data availability

The full dataset shown in the figures and tables is publicly available at https://doi.org/10.5281/zenodo.4048589. Source data are provided with this paper.

Code availability

The standard CAMx model (version 6.3) is an open source model and free to download at http://www.camx.com/. The modified module with split OA sources (PSI-VBS) is available at https://doi.org/10.5281/zenodo.3540826.

32. Canagaratna, M. et al. Chemical and microphysical characterization of ambient aerosols with the aerodyne aerosol mass spectrometer. *Mass Spectrom. Rev.* **26**, 185–222 (2007).
33. Allan, J. D. et al. Quantitative sampling using an Aerodyne aerosol mass spectrometer. 1. Techniques of data interpretation and error analysis. *J. Geophys. Res. Atmos.* **108**, https://doi.org/10.1029/2002JD002358 (2003).
34. Waked, A. et al. Source apportionment of PM10 in a north-western Europe regional urban background site (Lens, France) using positive matrix factorization and including primary biogenic emissions. *Atmos. Chem. Phys.* **14**, 3325–3346 (2014).
35. Albinet, A., Tomaz, S. & Lestremau, F. A really quick easy cheap effective rugged and safe (QuEChERS) extraction procedure for the analysis of particle-bound PAHs in ambient air and emission samples. *Sci. Total Environ.* **450/451**, 31–38 (2013).
36. Albinet, A., Nalin, F., Tomaz, S., Beaumont, J. & Lestremau, F. A simple QuEChERS-like extraction approach for molecular chemical characterization of organic aerosols: application to nitrated and oxygenated PAH derivatives (NPAH and OPAH) quantified by GC–NICIMS. *Anal. Bioanal. Chem.* **406**, 3131–3148 (2014).
37. Srivastava, D. et al. Speciation of organic fractions does matter for aerosol source apportionment. Part 2: Intensive short-term campaign in the Paris area (France). *Sci. Total Environ.* **634**, 267–278 (2018).
38. Verlhac, S. & Albinet, A. European interlaboratory comparison for the analysis of PAH in ambient air. http://www.lcsqa.org/rapport/2015/ineris/european-interlaboratory-comparison-for-the-analysis-of-pah-in-ambient-air (LCSQA, 2015).
39. Samaké, A. et al. Polyols and glucose particulate species as tracers of primary biogenic organic aerosols at 28 French sites. *Atmos. Chem. Phys.* **19**, 3357–3374 (2019).
40. Nozière, B. et al. The molecular identification of organic compounds in the atmosphere: state of the art and challenges. *Chem. Rev.* **115**, 3919–3983 (2015).
41. Birch, M. & Cary, R. Elemental carbon-based method for monitoring occupational exposures to particulate diesel exhaust. *Aerosol Sci. Technol.* **25**, 221–241 (1996).
42. Cavalli, F., Viana, M., Yttri, K. E., Genberg, J. & Putaud, J.-P. Toward a standardised thermal-optical protocol for measuring atmospheric organic and elemental carbon: the EUSAAR protocol. *Atmos. Meas. Tech.* **3**, 79–89 (2010).
43. Piazzalunga, A., Bernardoni, V., Fermo, P. & Vecchi, R. Optimisation of analytical procedures for the quantification of ionic and carbonaceous fractions in the atmospheric aerosol and applications to ambient samples. *Anal. Bioanal. Chem.* **405**, 1123–1132 (2013).
44. Jaffrezo, J., Calas, N. & Bouchet, M. Carboxylic acids measurements with ionic chromatography. *Atmos. Environ.* **32**, 2705–2708 (1998).
45. Calas, A. et al. Comparison between five acellular oxidative potential measurement assays performed with detailed chemistry on PM 10 samples from the city of Chamonix (France). *Atmos. Chem. Phys.* **18**, 7863–7875 (2018).
46. Foucaud, L., Wilson, M., Brown, D. & Stone, V. Measurement of reactive species production by nanoparticles prepared in biologically relevant media. *Toxicol. Lett.* **174**, 1–9 (2007).
47. Zhou, J. et al. Development, characterization and first deployment of an improved online reactive oxygen species analyzer. *Atmos. Meas. Tech.* **11**, 65–80 (2018).
48. Zhou, J. et al. Particle-bound reactive oxygen species (PB-ROS) emissions and formation pathways in residential wood smoke under different combustion and aging conditions. *Atmos. Chem. Phys.* **18**, 6985–7000 (2018).
49. Charrier, J. G. et al. Oxidant production from source-oriented particulate matter. Part 1: Oxidative potential using the dithiothreitol (DTT) assay. *Atmos. Chem. Phys.* **15**, 2327–2340 (2015).
50. Cho, A. K. et al. Redox activity of airborne particulate matter at different sites in the Los Angeles Basin. *Environ. Res.* **99**, 40–47 (2005).
51. Mudway, I. S. et al. An in vitro and in vivo investigation of the effects of diesel exhaust on human airway lining fluid antioxidants. *Arch. Biochem. Biophys.* **423**, 200–212 (2004).
52. Huang, W. et al. Optimization of the measurement of particle-bound reactive oxygen species with 2′, 7′-dichlorofluorescin (DCFH). *Wat. Air Soil Pollut.* **227**, 164 (2016).
53. Künzi, L. et al. Toxicity of aged gasoline exhaust particles to normal and diseased airway epithelia. *Sci. Rep.* **5**, 11801 (2015).
54. Paatero, P. & Tapper, U. Positive matrix factorization: a non-negative factor model with optimal utilization of error estimates of data values. *Environmetrics* **5**, 111–126 (1994).
55. Paatero, P. The multilinear engine—a table-driven, least squares program for solving multilinear problems, including the n-way parallel factor analysis model. *J. Comput. Graph. Stat.* **8**, 854–888 (1999).
56. Canonaco, F., Crippa, M., Slowik, J., Baltensperger, U. & Prévôt, A. SoFi, an IGOR-based interface for the efficient use of the generalized multilinear engine (ME-2) for the source apportionment: ME-2 application to aerosol mass spectrometer data. *Atmos. Meas. Tech.* **6**, 3649–3661 (2013).
57. Crippa, M. et al. Identification of marine and continental aerosol sources in Paris using high resolution aerosol mass spectrometry. *J. Geophys. Res. Atmos.* **118**, 1950–1963 (2013).
58. Bozzetti, C. et al. Size-resolved identification, characterization, and quantification of primary biological organic aerosol at a European rural site. *Environ. Sci. Technol.* **50**, 3425–3434 (2016).
59. Amato, F. et al. Traffic induced particle resuspension in Paris: emission factors and source contributions. *Atmos. Environ.* **129**, 114–124 (2016).
60. Yang, A. et al. Children's respiratory health and oxidative potential of PM2. 5: the PIAMA birth cohort study. *Occup. Environ. Med.* **73**, 154–160 (2016).
61. Fang, T. et al. Oxidative potential of ambient water-soluble PM2.5 in the southeastern United States: contrasts in sources and health associations between ascorbic acid (AA) and dithiothreitol (DTT) assays. *Atmos. Chem. Phys.* **16**, 3865–3879 (2016).
62. Bates, J. T. et al. Reactive oxygen species generation linked to sources of atmospheric particulate matter and cardiorespiratory effects. *Environ. Sci. Technol.* **49**, 13605–13612 (2015).

63. Yang, A. et al. Agreement of central site measurements and land use regression modeled oxidative potential of PM2.5 with personal exposure. *Environ. Res.* **140**, 397–404 (2015).
64. Yanosky, J. D., Tonne, C. C., Beevers, S. D., Wilkinson, P. & Kelly, F. J. Modeling exposures to the oxidative potential of PM10. *Environ. Sci. Technol.* **46**, 7612–7620 (2012).
65. Perrone, M. G. et al. PM chemical composition and oxidative potential of the soluble fraction of particles at two sites in the urban area of Milan, Northern Italy. *Atmos. Environ.* **128**, 104–113 (2016).
66. Szigeti, T. et al. Changes in chemical composition and oxidative potential of urban PM2.5 between 2010 and 2013 in Hungary. *Sci. Total Environ.* **518/519**, 534–544 (2015).
67. Ntziachristos, L., Froines, J. R., Cho, A. K. & Sioutas, C. Relationship between redox activity and chemical speciation of size-fractionated particulate matter. *Part. Fibre Toxicol.* **4**, 5 (2007).
68. Shirmohammadi, F. et al. Fine and ultrafine particulate organic carbon in the Los Angeles basin: trends in sources and composition. *Sci. Total Environ.* **541**, 1083–1096 (2016).
69. Shafer, M. M., Hemming, J. D. C., Antkiewicz, D. S. & Schauer, J. J. Oxidative potential of size-fractionated atmospheric aerosol in urban and rural sites across Europe. *Faraday Discuss.* **189**, 381–405 (2016).
70. Verma, V. et al. Organic aerosols associated with the generation of reactive oxygen species (ROS) by water-soluble PM2.5. *Environ. Sci. Technol.* **49**, 4646–4656 (2015).
71. Weber, S. et al. An apportionment method for the oxidative potential of atmospheric particulate matter sources: application to a one-year study in Chamonix, France. *Atmos. Chem. Phys.* **18**, 9617–9629 (2018).
72. Kramer, A. J. et al. Assessing the oxidative potential of isoprene-derived epoxides and secondary organic aerosol. *Atmos. Environ.* **130**, 211–218 (2016).
73. Wang, S. et al. Relationship between chemical composition and oxidative potential of secondary organic aerosol from polycyclic aromatic hydrocarbons. *Atmos. Chem. Phys.* **18**, 3987–4003 (2018).
74. Saffari, A. et al. Impact of primary and secondary organic sources on the oxidative potential of quasi-ultrafine particles (PM0.25) at three contrasting locations in the Los Angeles Basin. *Atmos. Environ.* **120**, 286–296 (2015).
75. Tong, H. et al. Reactive oxygen species formed by secondary organic aerosols in water and surrogate lung fluid. *Environ. Sci. Technol.* **52**, 11642–11651 (2018).
76. Lovett, C., Sowlat, M. H., Saliba, N. A., Shihadeh, A. L. & Sioutas, C. Oxidative potential of ambient particulate matter in Beirut during Saharan and Arabian dust events. *Atmos. Environ.* **188**, 34–42 (2018).
77. Jiang, H. & Jang, M. Dynamic oxidative potential of atmospheric organic aerosol under ambient sunlight. *Environ. Sci. Technol.* **52**, 7496–7504 (2018).
78. Tuet, W. Y. et al. Chemical oxidative potential of secondary organic aerosol (SOA) generated from the photooxidation of biogenic and anthropogenic volatile organic compounds. *Atmos. Chem. Phys.* **17**, 839–853 (2017).
79. McWhinney, R., Zhou, S. & Abbatt, J. Naphthalene SOA: redox activity and naphthoquinone gas–particle partitioning. *Atmos. Chem. Phys.* **13**, 9731–9744 (2013).
80. Chung, M. Y. et al. Aerosol-borne quinones and reactive oxygen species generation by particulate matter extracts. *Environ. Sci. Technol.* **40**, 4880–4886 (2006).
81. Lakey, P. S. et al. Chemical exposure-response relationship between air pollutants and reactive oxygen species in the human respiratory tract. *Sci. Rep.* **6**, 32916 (2016).
82. Huang, R.-J. et al. High secondary aerosol contribution to particulate pollution during haze events in China. *Nature* **514**, 218–222 (2014).
83. Hildebrandt Ruiz, L. & Yarwood, G. *Interactions Between Organic Aerosol And NOy: Influence On Oxidant Production*. http://aqrp.ceer.utexas.edu/projectinfoFY12_13%5C12-012%5C12-012%20Final%20Report.pdf (University of Texas at Austin and ENVIRON International Corporation, 2013).
84. Nenes, A., Pandis, S. N. & Pilinis, C. ISORROPIA: a new thermodynamic equilibrium model for multiphase multicomponent inorganic aerosols. *Aquat. Geochem.* **4**, 123–152 (1998).
85. Koo, B., Knipping, E. & Yarwood, G. 1.5-dimensional volatility basis set approach for modeling organic aerosol in CAMx and CMAQ. *Atmos. Environ.* **95**, 158–164 (2014).
86. Ciarelli, G. et al. Modelling winter organic aerosol at the European scale with CAMx: evaluation and source apportionment with a VBS parameterization based on novel wood burning smog chamber experiments. *Atmos. Chem. Phys.* **17**, 7653–7669 (2017).
87. Jiang, J. et al. Effects of two different biogenic emission models on modelled ozone and aerosol concentrations in Europe. *Atmos. Chem. Phys.* **19**, 3747–3768 (2019).
88. Platt, S. M. et al. Gasoline cars produce more carbonaceous particulate matter than modern filter-equipped diesel cars. *Sci. Rep.* **7**, 4926 (2017).
89. Kuenen, J., Visschedijk, A., Jozwicka, M. & Denier Van Der Gon, H. TNO-MACC_II emission inventory; a multi-year (2003–2009) consistent high-resolution European emission inventory for air quality modelling. *Atmos. Chem. Phys.* **14**, 10963–10976 (2014).
90. Emmons, L. K. et al. Description and evaluation of the Model for Ozone and Related chemical Tracers, version 4 (MOZART-4). *Geosci. Model Dev.* **3**, 43–67 (2010).
91. Fernandes, A. et al. Comparisons of aerosol optical depth provided by seviri satellite observations and CAMx air quality modelling. In *36th Int. Symp. on Remote Sensing of Environment* Vol. 47, 187–193 (International Archives of the Photogrammetry Remote Sensing and Spatial Information Sciences, 2015).
92. Denjean, C. et al. Size distribution and optical properties of mineral dust aerosols transported in the western Mediterranean. *Atmos. Chem. Phys.* **16**, 1081–1104 (2016).
93. Hulskotte, J., van der Gon, H. D., Visschedijk, A. & Schaap, M. Brake wear from vehicles as an important source of diffuse copper pollution. *Water Sci. Technol.* **56**, 223–231 (2007).
94. Tørseth, K. et al. Introduction to the European Monitoring and Evaluation Programme (EMEP) and observed atmospheric composition change during 1972–2009. *Atmos. Chem. Phys.* **12**, 5447–5481 (2012).
95. Aas, W. & Breivik, K. *Heavy Metals and POP Measurements, 2011*. EMEP/CCC-Report 4/2013, https://projects.nilu.no/ccc/reports/cccr4-2013.pdf (European Monitoring and Evaluation Programme, 2013).
96. Crippa, M. et al. Organic aerosol components derived from 25 AMS data sets across Europe using a consistent ME-2 based source apportionment approach. *Atmos. Chem. Phys.* **14**, 6159–6176 (2014).
97. Putaud, J.-P. et al. A European aerosol phenomenology. 3: Physical and chemical characteristics of particulate matter from 60 rural, urban, and kerbside sites across Europe. *Atmos. Environ.* **44**, 1308–1320 (2010).
98. Charron, A. et al. Identification and quantification of particulate tracers of exhaust and non-exhaust vehicle emissions. *Atmos. Chem. Phys.* **19**, 5187–5207 (2019).
99. European Chemicals Agency *Default Human Factor Values For Use In Exposure Assessments For Biocidal Products. Recommendation no. 14 of the BPC Ad hoc Working Group on Human Exposure* https://echa.europa.eu/documents/10162/21664016/recom_14+_default+human_factor_values_biocidal+products_en.pdf/88354d31-8a3a-475a-9c7d-d8ef8088d004 (ECHA, accessed 12 June 2017).
100. United States Environmental Protection Agency *A Summary of The Recommended Values From the Exposure Factors Handbook: 2011 Edition* https://www.epa.gov/expobox/exposure-assessment-tools-approaches-indirect-estimation-scenario-evaluation#factors (EPA, 2011).
101. Miller, F. J., Asgharian, B., Schroeter, J. D. & Price, O. Improvements and additions to the multiple path particle dosimetry model. *J. Aerosol Sci.* **99**, 14–26 (2016).
102. Amann, M. et al. Cost-effective control of air quality and greenhouse gases in Europe: modeling and policy applications. *Environ. Model. Softw.* **26**, 1489–1501 (2011).
103. Leni, Z. et al. Oxidative stress-induced inflammation in susceptible airways by anthropogenic aerosol. *PLoS One* pone.0233425 (2020).
104. National Center for Atmospheric Research. *Weather Research and Forecasting Model WRF-ARW Version 3 Modeling System User's Guide* (NCAR, 2016).

Acknowledgements We thank the Swiss Federal Office of Environment; Liechtenstein; Ostluft; and the Swiss cantons Basel, Graubünden and Thurgau. We also thank AWEL Zurich for providing us with samples collected in Islisbergtunnel. For the air-quality modelling, we thank the TNO for providing anthropogenic emissions, the European Centre for Medium-Range Weather Forecasts (ECMWF) for access to the meteorological data, National Center for Atmospheric Research (NCAR) for the initial and boundary conditions, the European Environmental Agency (EEA) for the air-quality data and the Swiss National Supercomputing Centre (CSCS). The support by Ramboll for the CAMx model is gratefully acknowledged. We acknowledge the Swiss Federal Laboratories for Materials Science and Technology (Empa) and the National Air Pollution Monitoring Network (NABEL) for providing air-quality data. We acknowledge the use of country borders from https://thematicmapping.org/downloads/world_borders.php shared under a Creative Commons Attribution-Share Alike license. We thank N. Marchand for scientific discussions. K.R.D. acknowledges support by VULCAIN and Swiss National Science Foundation mobility grant P2EZP2_181599. M.G. and J.D. acknowledge financial support by the Swiss National Science Foundation grant CR32I3_166325. A.A. and O.F. acknowledge financial support by the French Ministry of Environment. G.U. and J.L.J. thank the programmes LEFE CHAT (grant 863353), LABEX OSUG@2020 (ANR-10-LABX-56), ANR-19-CE34-0002-01, and the " Investissements d'avenir" programme (ANR-15-IDEX-02) for supporting this work and funding analytical instruments.

Author contributions K.R.D., I.E.H. and A.S.H.P. designed the research. G.U. performed the OP measurements. K.R.D., G.S. and A.V. performed the offline aerosol mass spectrometer measurements. J.-L.J. measured the organic markers. A.A. measured the polyaromatic hydrocarbons and oxy-polyaromatic hydrocarbons (quinones). Z.L., L.-E.C. and M.G. performed the toxicological experiments. J.J., S.A., K.R.D. and I.E.H. performed the air-quality and OP modelling. A.S. and M.S. performed the TNO model runs. J.J.P.K. and M.S. provided emission data. S.W., O.F. and G.U. provided OP data for model validation. F.C. provided analytical software for source apportionment. K.R.D., J.J. and I.E.H. performed the data analysis. K.R.D., G.U., J.J., L.-E.C., A.V., G.S., F.C., A.S., M.S., A.A., S.A., J.D., U.B., I.E.H., J.-L.J. and A.S.H.P. interpreted the results and wrote the manuscript.

Competing interests The authors declare no competing interests.

Additional information

Supplementary information is available for this paper at https://doi.org/10.1038/s41586-020-2902-8.

Correspondence and requests for materials should be addressed to J.J., I.E.H. or A.S.H.P.

Peer review information *Nature* thanks Flemming Cassee, Ally Lewis and the other, anonymous, reviewer(s) for their contribution to the peer review of this work.

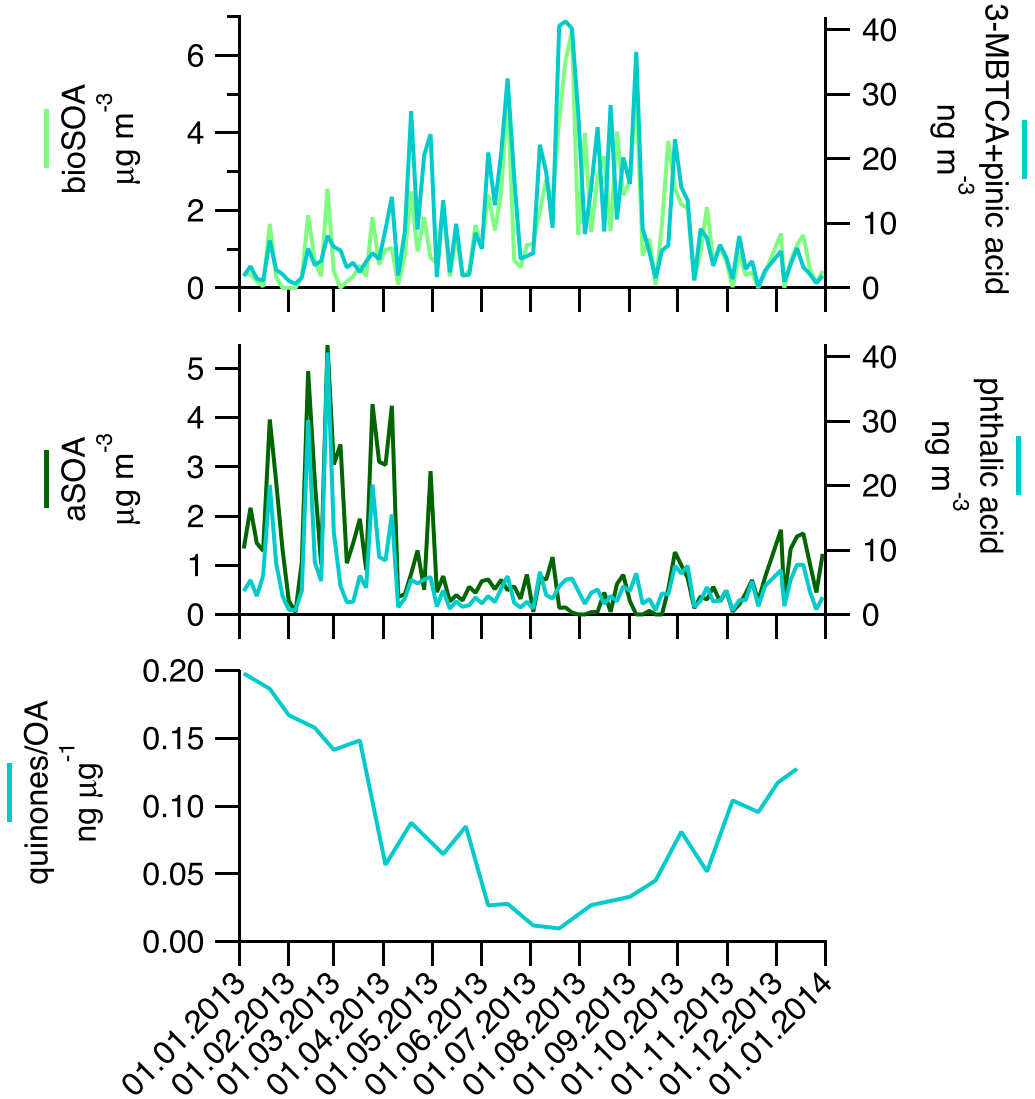

Extended Data Fig. 1 | Seasonal variability of SOA types, their markers and quinones. Concentration time series (every fourth day) of bioSOA and the sum of 3-MBTCA and pinic acid (both oxidation products of terpenes), aSOA and phthalic acid (an oxidation product of naphthalene and methyl-naphthalenes), as well as time series (bimonthly) of the mass fraction of polyaromatic quinones of OA in Frauenfeld.

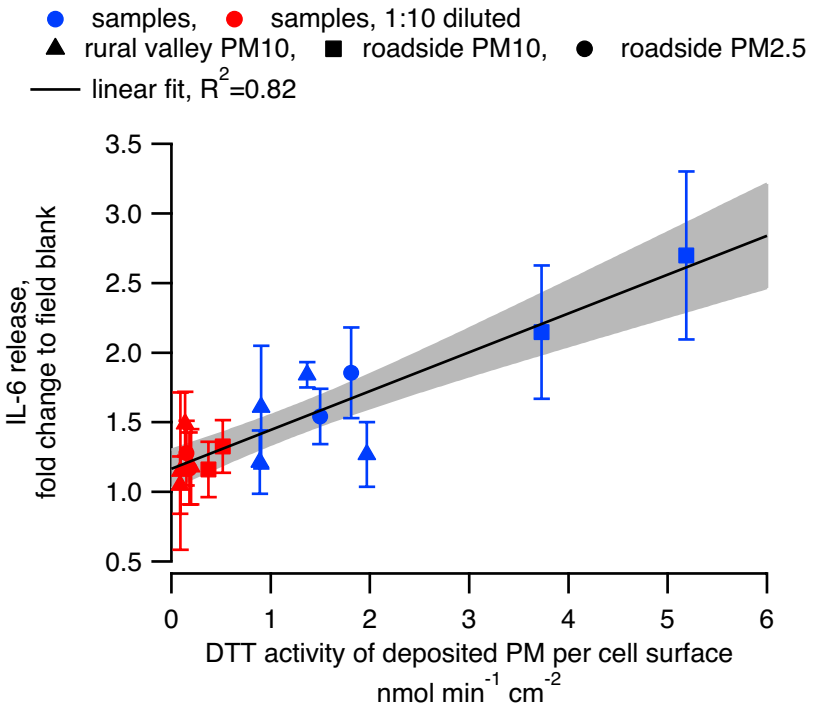

Extended Data Fig. 2 | Cellular response to exposure to PM with varying OP activity. Comparison between IL-6 release (fold change to field blank) in re-differentiated human bronchial epithelia exposed to filter extracts and DTT activity of the deposited PM per cell surface. The error bars represent the standard error of replicate experiments. The relative errors for DTT per cell surface are in comparison to IL-6 release five to ten times smaller and are therefore not displayed. A linear regression (IL-6 release = (1.17 ± 0.14) × DTT per cell surface + (0.28 ± 0.07)) is displayed (grey line) with 95% confidence interval (grey-shaded area). More detailed comparisons between the cellular responses to deposited PM are presented in Leni et al.[103].

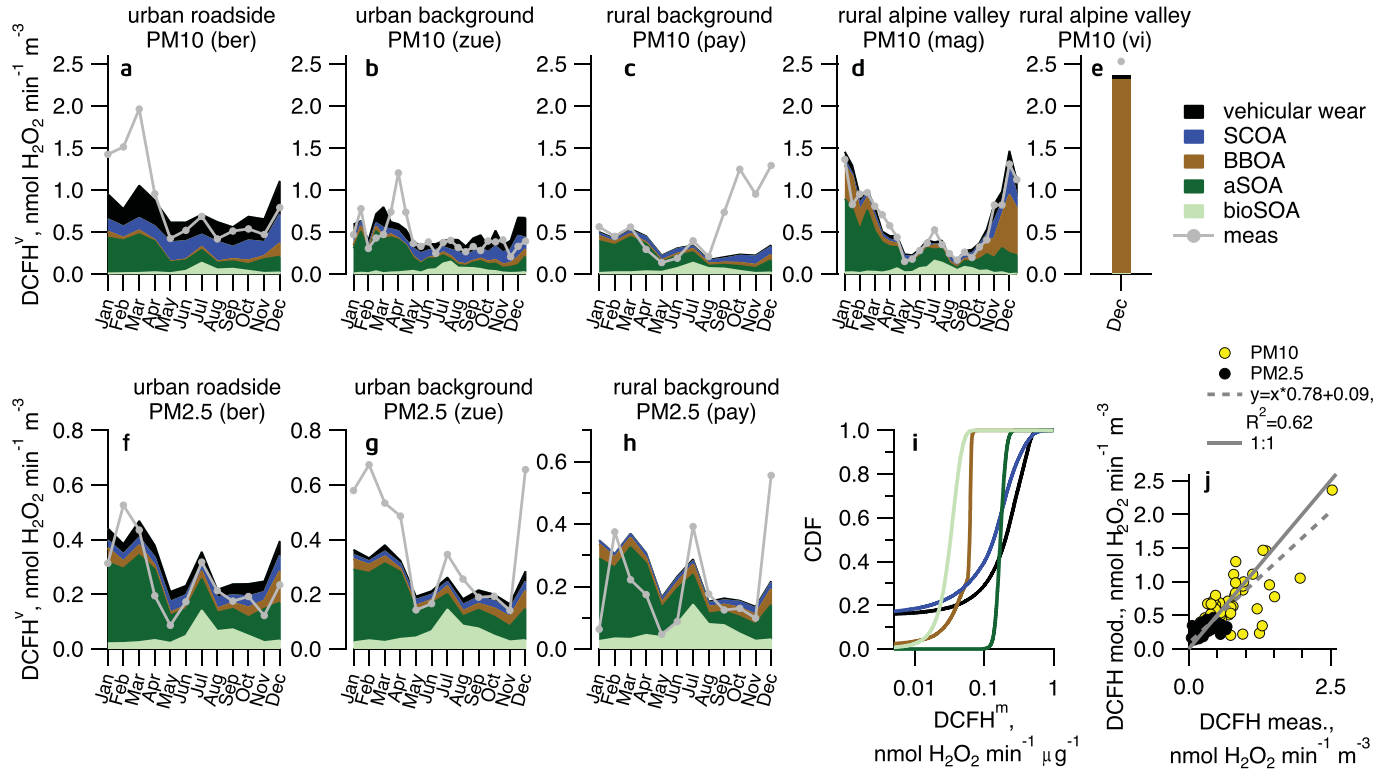

Extended Data Fig. 3 | DCFH^v sources at rural and urban measurement sites. Contributions of metal (crustal, vehicular wear, residential heating) and OA (SCOA, HOA, COA, BBOA, aSOA, bioSOA) sources and other PM components to $DCFH^v_{PM10}$ and $DCFH^v_{PM2.5}$ at five sites with different emission characteristics (109 composite samples): **a** and **f**, urban roadside (ber, Bern Bollwerk); **b** and **g**, urban background (zue, Zurich Kaserne); **c** and **h**, rural background (pay, Payerne MeteoSuisse); **d**, rural alpine valley (mag, Magadino-Cadenazzo); **e**, wintertime pollution episode in alpine valley (vi, S. Vittore Center); **i**, $DCHF^m$ of contributing metal and OA sources; and **j**, comparison between modelled (mod.) and measured $DCHF^v$.

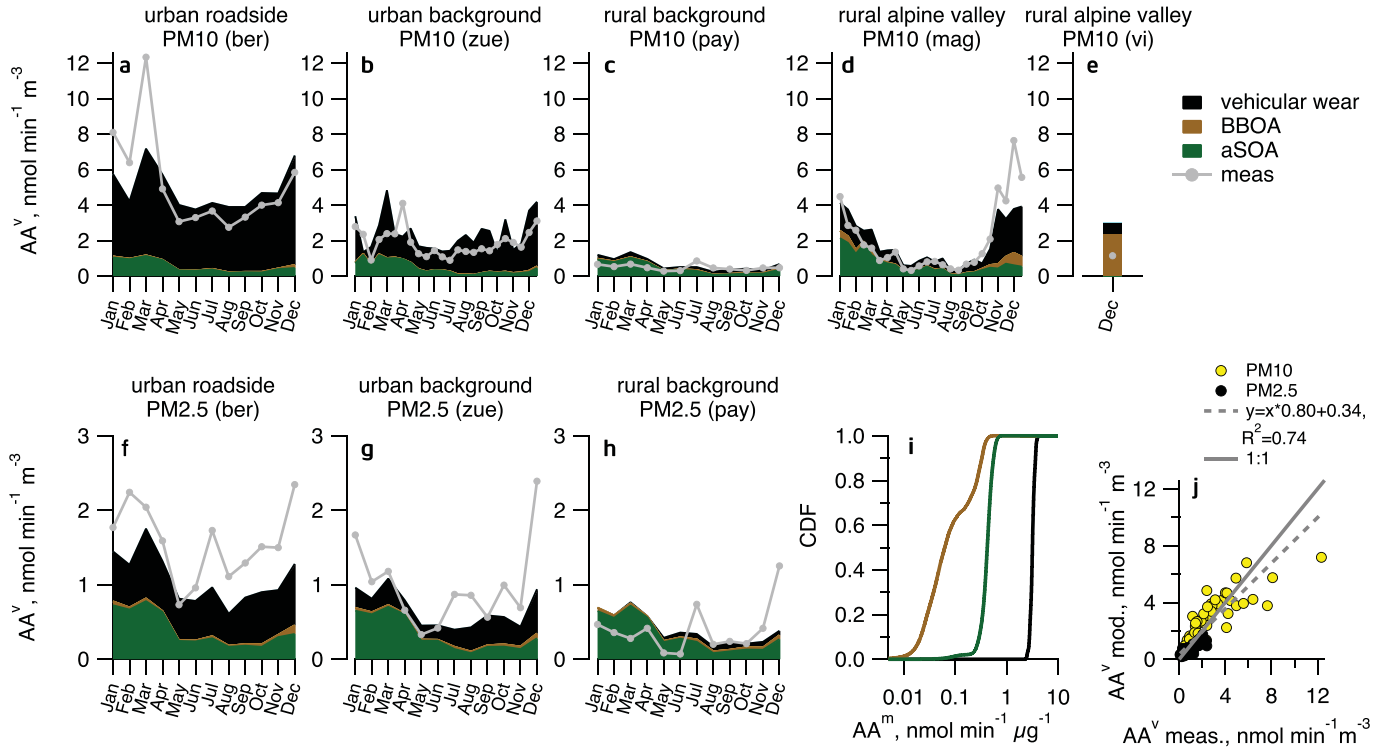

Extended Data Fig. 4 | AA^v sources at rural and urban measurement sites. Contributions of metal (crustal, vehicular wear, residential heating) and OA (SCOA, HOA, COA, BBOA, aSOA, bioSOA) sources and other PM components to AA^v_{PM10} and $AA^v_{PM2.5}$ at five sites with different emission characteristics (109 composite samples): **a** and **f**, urban roadside; **b** and **g**, urban background; **c** and **h**, rural background; **d**, rural alpine valley; **e**, wintertime pollution episode in alpine valley; **i**, AA^v of contributing metal and OA sources; and **j**, comparison between modelled and measured AA^v.

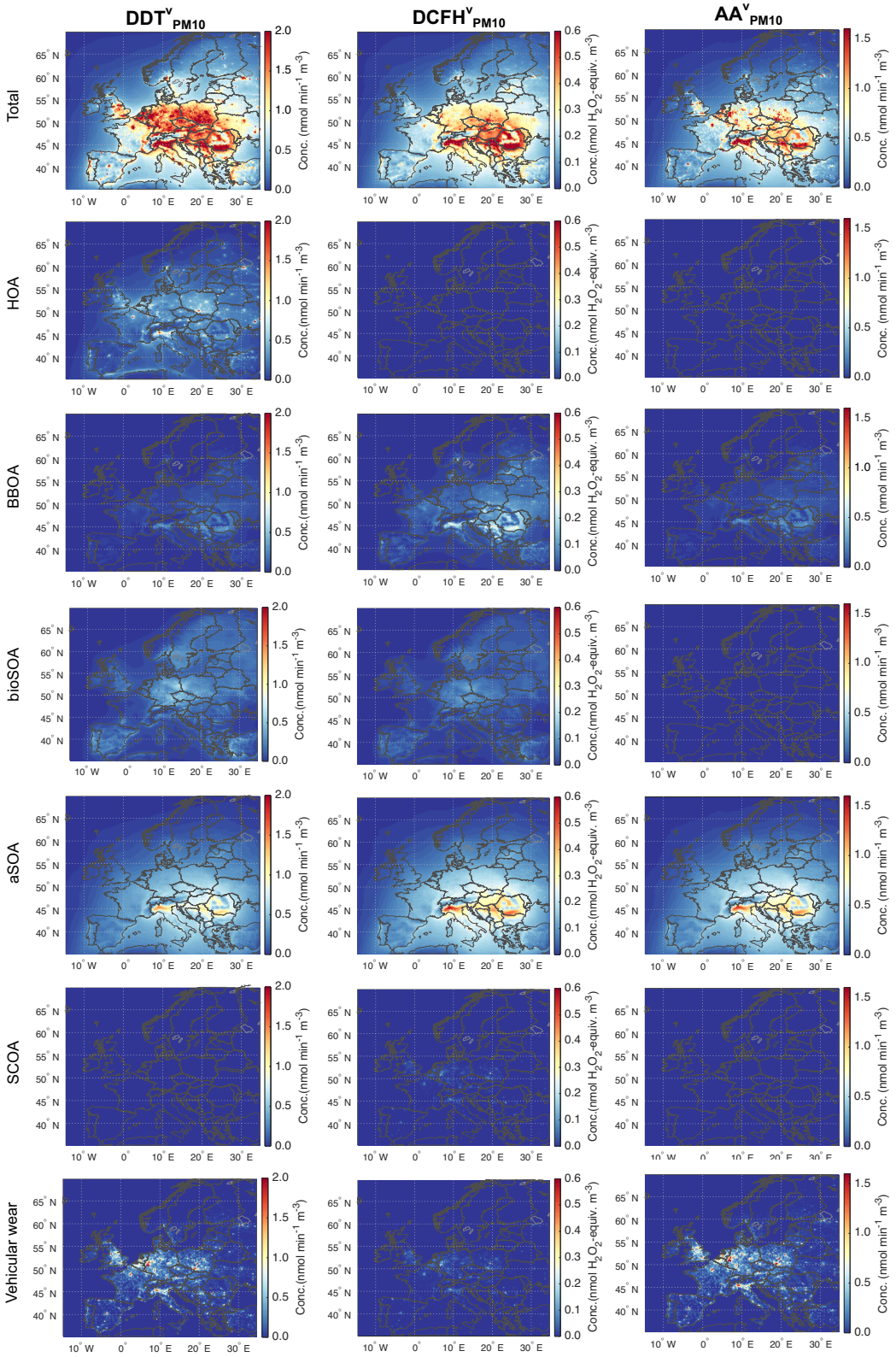

Extended Data Fig. 5 | Source contributions to different OP^{v} assays. The modelled total DTT$^{v}_{PM10}$, DCFH$^{v}_{PM10}$ and AA$^{v}_{PM10}$ (top row) and the contributions of the relevant sources (lower rows) (chosen in the multiple linear regression model): traffic POA (HOA), biomass-burning POA (BBOA), biogenic SOA (bioSOA), anthropogenic SOA (aSOA), coarse organic vehicular emissions (SCOA), and coarse inorganic/metal vehicular emissions (vehicular wear).

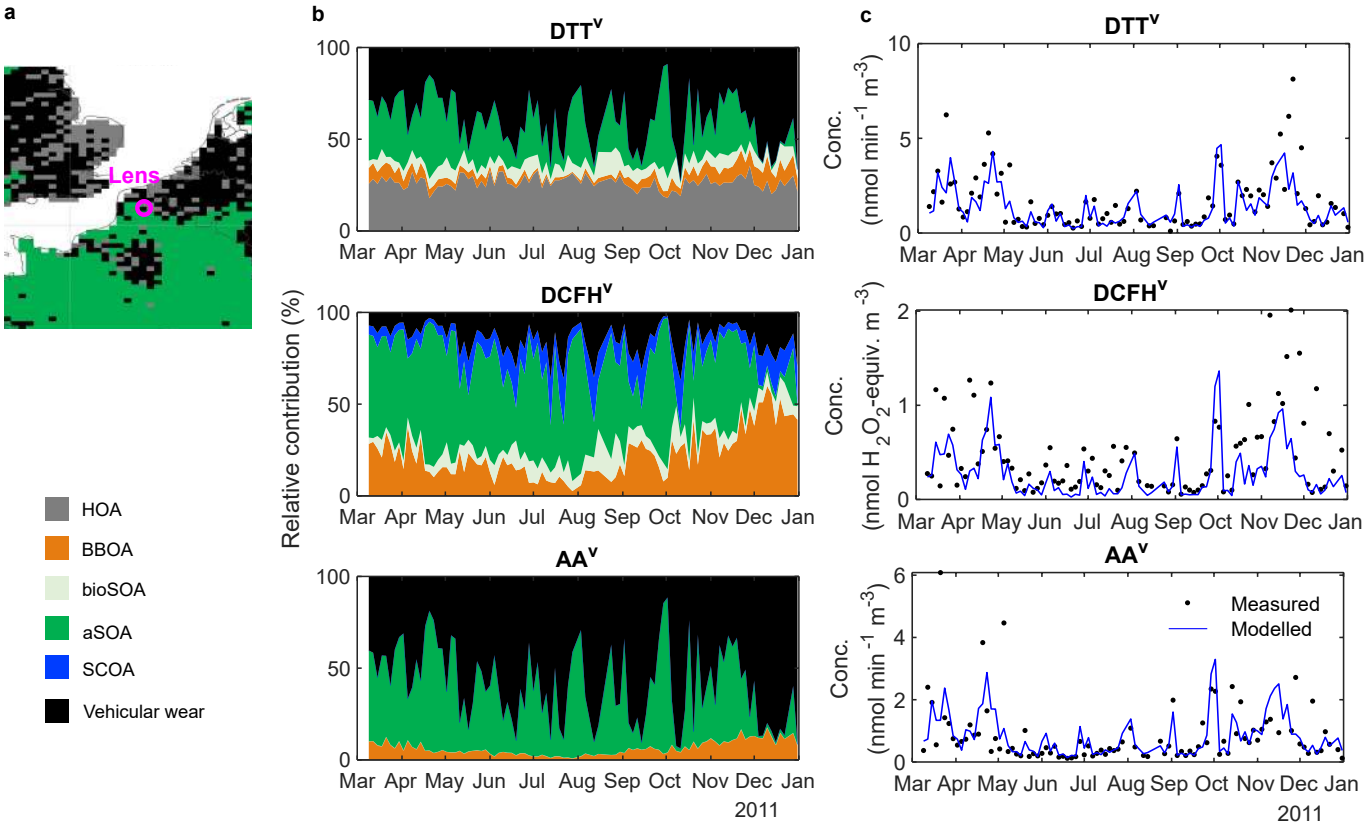

Extended Data Fig. 6 | Validation of OP^{v} modelling results. Detailed comparison between measured and modelled OP at Lens for the three essays investigated here (DTT, DCFH and AA). **a**, location of Lens along with the dominating DTT source; **b**, modelled contributions of the different sources to OP; and **c**, comparison between modelled and measured OP.

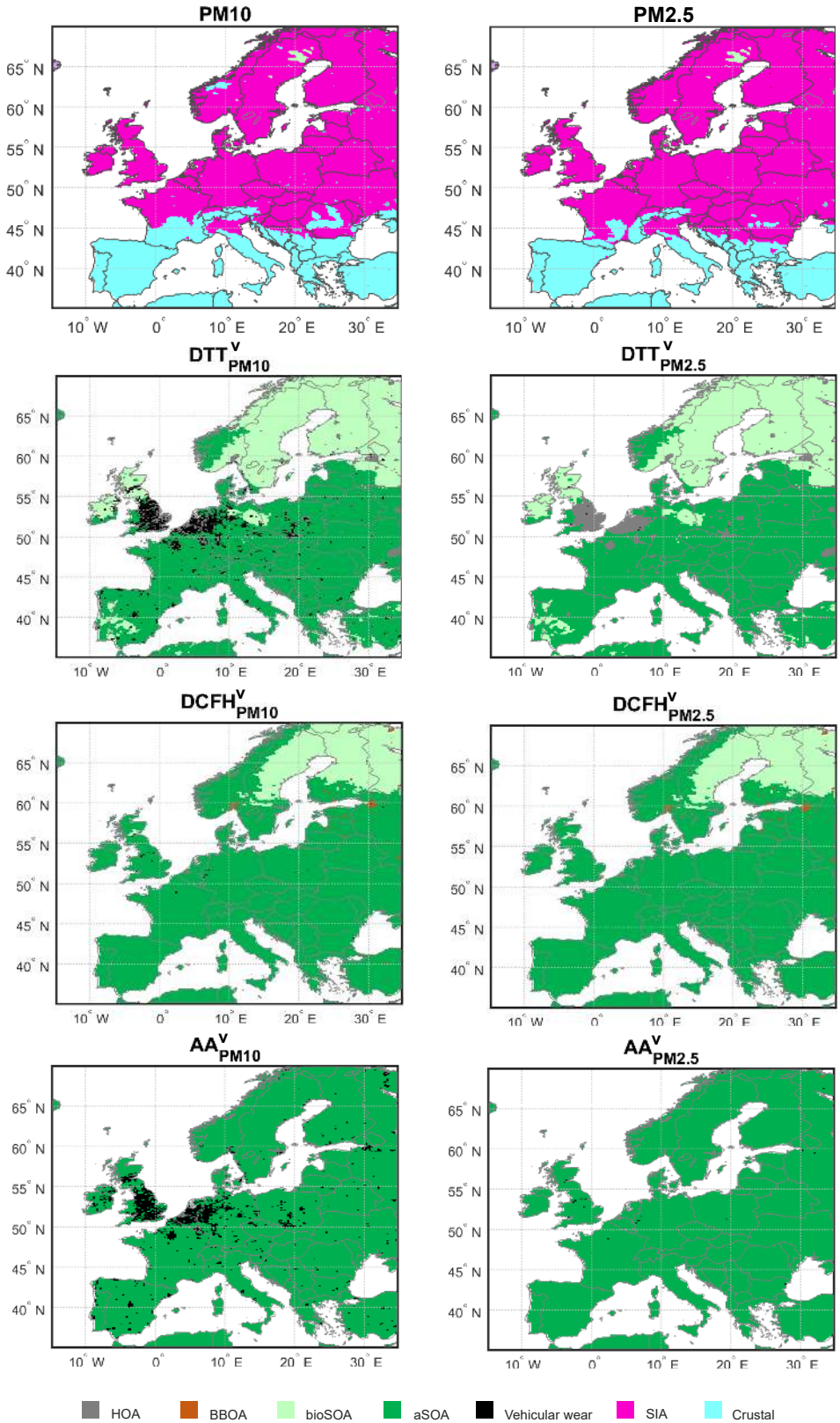

Extended Data Fig. 7 | Largest contributing sources to OP^{v} and PM mass concentrations in Europe. Largest contributors to OP^{v} in PM_{10} (DTT^{v}, DCFH^{v}, AA^{v}) in each grid cell over land surface in the modelled area for PM_{10} and $PM_{2.5}$.

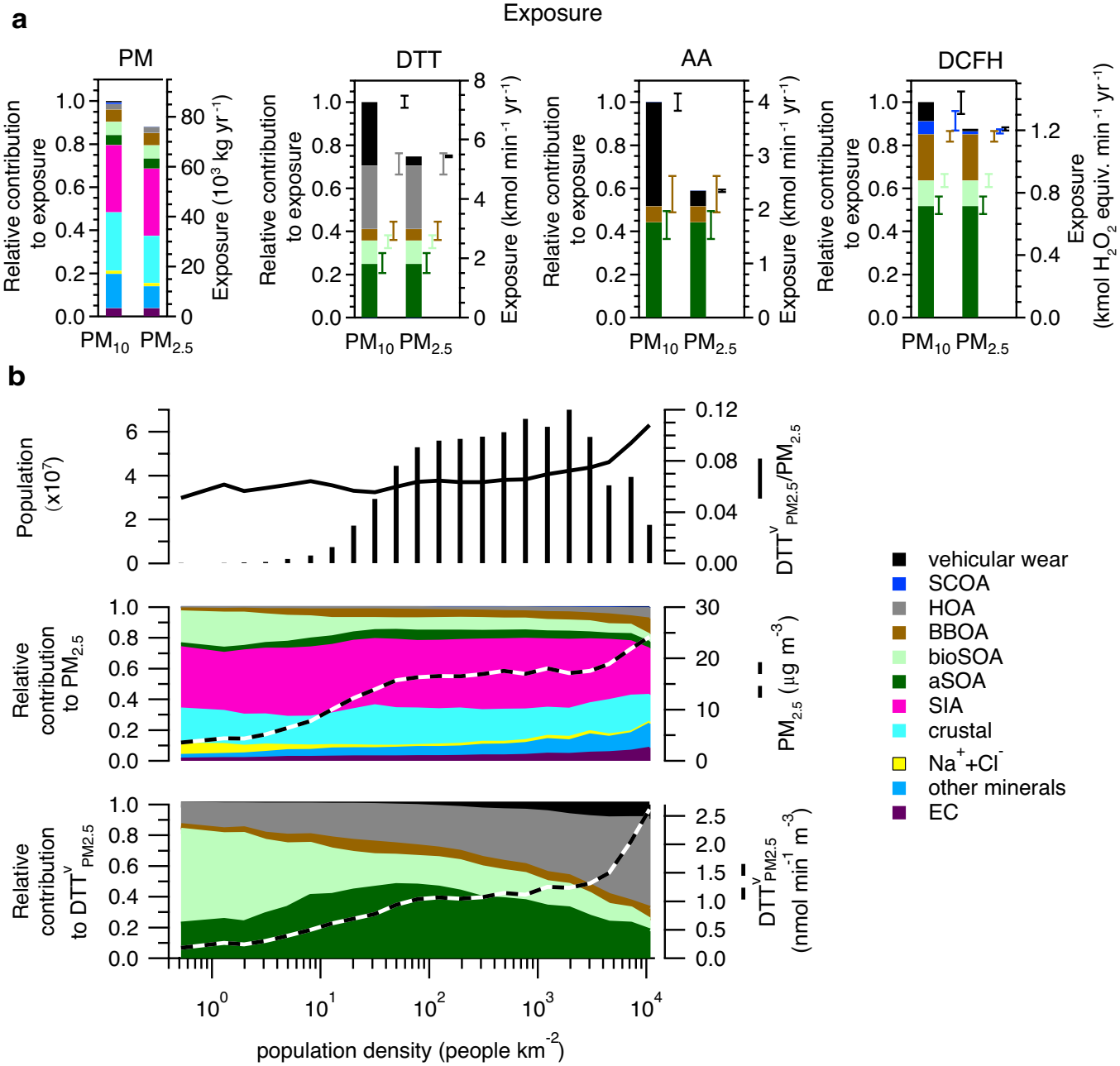

Extended Data Fig. 8 | Source contributions to PM and OP exposure, and their dependence on population density for PM2.5 and $OP^v_{PM2.5}$. a, Contributions of aerosol sources and components to the total PM, DTT, DCFH and AA exposure for both PM_{10} and $PM_{2.5}$ in Europe (relative contributions to the respective exposure and absolute exposure, copied from Fig. 3a). Exposures are computed as population integrated amount of OP^v or PM in inhaled ambient air accumulated over a full year. Error bars depict the range between the 25% and 75% quartiles obtained from the Monte Carlo analysis propagating the uncertainty of OP^m of the single sources from the multiple linear regression model. **b**, $DTT^v_{PM2.5}/PM_{2.5}$ and population (top), $PM_{2.5}$ concentrations and relative source contributions to $PM_{2.5}$ (middle), and relative source contributions to $DTT^v_{PM2.5}$ and $DTT^v_{PM2.5}$ (bottom) in comparison to the population density in the modelled domain. We note that data for $PM_{2.5}$ are shown here, while Fig. 3b shows data for PM_{10}.